明志科技大學
MING CHI UNIVERSITY OF TECHNOLOGY

Master's Program of the Department of Electronic Engineering

Master Thesis

A Study on Exciplex Host Towards Improving Emission Efficiency of Phosphorescent Organic Light-emitting Diodes

Graduate Student: Kevin Sutanto

Advisor: Shun-Wei Liu, Ph.D

January 2022

Ming Chi University of Technology
Recommendation Letter from the Thesis Advisor

This thesis is by Kevin Sutanto of the Department of Electronic Engineering, entitled: A Study on Exciplex Host Towards Improving Emission Efficiency of Phosphorescent Organic Light-emitting Diodes, which is written under my supervision and I agree to propose it for examination.

Advisor Shun-Wei Liu (Signature)

11 / 29 / 2021 (mm/dd/yyyy)

Ming Chi University of Technology
Thesis/Dissertation Oral Defense Committee Certification

This thesis is by Kevin Sutanto of the Master's Program of the Department of Electronic Engineering, entitled: A Study on Exciplex Host Towards Improving Emission Efficiency of Phosphorescent Organic Light-emitting Diodes, who is qualified for master/doctorate degree through the verification of the committee.

Convener of the degree examination committee Chih-Hao Chang (Signature)

Committee members Shun-Wei Liu

Chih-Hao Chang

Sajal Biring

Department Chair Ya-Fen Wu

01 / 06 / 2022 (mm/dd/yyyy)

Abstract

The first practical organic light-emitting diodes proposed by Tang *et al.* have attracted lot of attention to realize OLED applications. Along with the improvement of OLEDs, high electroluminescence is needed for successful OLED applications. Reaching 100% internal quantum efficiency by fully harvesting the light can be achievable with the utilization of phosphorescent dopants. In other ways, exciplex as a co-host system can be used to achieve highly efficient OLED.

In this work, the optimization of OLED devices using various exciplex systems blended with a novel synthesized phosphorescent dopant has been studied. The bulk exciplex formation was designed using two kinds of donor materials, BCzPh and TCTA, mixed with two kinds of acceptor materials, CN-T2T and B3PYMPM. The yellow and red phosphorescent dopant was synthesized by Tamkang University, Taiwan, with three types of dopants (Y1, R1, and R2). In yellow phosphorescent OLED with BCzPh system, the best exciplex system was shown by BCzPh:CN-T2T:4% Y1 exhibiting maximum external quantum efficiency of 20.02% with the maximum luminance of 72,640 cd m^{-2} at +8 V applied bias. In the TCTA exciplex system, the maximum EQE of 20.46% was achieved by TCTA:B3PYMPM:4% Y1. However, the maximum luminance shown in TCTA:CN-T2T:4% Y1 system is 68,260 cd m^{-2} at +8 V. For the red phosphorescent OLED, the devices show a low electroluminescence compared to other works, which needs a further study of the red phosphorescent dopant.

Keywords: *Phosphorescent OLED, phosphorescent dopant, bulk exciplex, external quantum efficieny, maximum luminance.*

Table of Contents

List of Figures

List of Tables

Chapter 1 Introduction

1.1 Overview

The emergence of the first practical organic light-emitting diodes by Tang *et al.* in 1987 has engaged the attention of a lot of researchers.[1] OLED (organic light-emitting diodes) becomes a very interesting topic due to their uniformity, lightweight, and flexibility.[2,3] In its development, the appearance of phosphorescent OLED makes a great improvement because of its ability to use both singlet and triplet exciton.[4] In theoretic, the phosphorescent OLED (PhOLED) can achieve 100% internal quantum efficiency (IQE).

In application, OLED has many advantages which can be a solution in visible light communication (VLC).[5] In visible light communication, yellow and red OLED are two colors which usually used. OLED has a fast dynamic response, low power consumption, and long lifetime. Besides that, the biggest advantage in VLC application is reducing much space compared with the conventional light source. Tailight in cars[6–8], automotive display technologies[9,10], traffic lights[5] are examples in VLC applications. The high device performance of OLED is needed to realize the implementation of OLED in visual light communication.

Figure 1.1 The application in automotive visual light communication[6–10]

The high performance of OLED has a high external quantum efficiency, high luminescence, low driving voltage, and low power consumption. One of the ways to improve the device performance was by utilization of exciplex forming co-host system.[11–16] Exciplex system was a co-host system that physically blended a donor (p-type) and acceptor (n-type). Achieving 100% internal quantum efficiency (IQE) is possible by an exciplex system with small differences in singlet and triplet states (ΔE_{ST}). The small ΔE_{ST} (0 – 0.5 eV) allows the triplet exciton to fall back to the singlet state through reverse intersystem crossing (RISC).[15,16] Furthermore, basically the donor and acceptor material is a transport material. Because of that, an exciplex system may achieve low driving voltage due to energy barrier-free between the transport and emission layer.[11] Shin *et al.* in 2018 show the exciplex-based host OLED has superior performance than a single host.[17] They have analyzed the mixing of carbazole-based hole transport host with CN-modified carbazole-based electron transport host. The result shows the exciplex-based (oCBP:CNmCBPCN) in blue phosphorescent OLED has a high external quantum efficiency (EQE) of 18.8% and a long lifetime of more than 1.8 times compared to the single host (CNmCBPCN).

On the other way, to improve the device performance is by modifying the structure of phosphorescent dopants. The best technique to modify phosphorescent dopants is using the heavy metal complexes as ion cores due to the strong spin-orbit coupling resulting in a non-radiative decay was reduced both of singlet and triplet exciton, and also reducing the waste exciton.[18] A lot of heavy metal complexes are usually used, which are iridium (Ir(III)),[18,19] platinum (Pt(II)),[20] palladium (Pd(II)),[20] cooper (Cu(I)),[21] gold (Au(III)),[22] etc. Among all, iridium(III) complexes have an exceptional behavior because of their good thermal and

chemical stability, high photoluminescence quantum yield (PLQY), and short phosphorescence lifetime.[19]

In the commercial market, the good electroluminescene performance of iridium-based yellow phosphorescent dopants is not too many choices. One of the best choices for yellow dopant is iridium(III)bis(4-phenylthieno[3,2-c] pyridinat o-N,C20)acetylacetonate or in commercial known as PO-01 dopant.[23–25] Lee *et al.* utilized this dopant (PO-01) mixed with phthalonitrile-based 3,3’’-di(9H-carbazol-9-yl)-[1,1’:2′,1’’-terphenyl]4′,5′-dicarbonitrile (IPNCz) host.[23] The highest EQE is 25.6 % and the maximum luminance (L_{max}) of 44,866 cd m^{-2} at voltage above +10 V. They also compared with the commercial host material 3,3′-Di(9H-carbazol-9-yl)-1,1′-biphenyl (mCBP) with 5% dopant concentration which achieved the EQE of 22.9 % and maximum luminance (L_{max}) of 44,226 cd m^{-2} at voltage above +10 V.

As a result of the lack of commercial yellow dopant options, many researchers trying to synthesis new iridium-based yellow phosphorescent dopants as an alternative way.[26–31] For example, Mei *et al.* in 2020 was successfully synthesized a yellow dopant by mixing iridium(III) metal complexes with thieno[2,3-d]pyridazine. The synthesized phosphorescent dopant was blended with single host material 4,4′-Bis(9-carbazolyl)-1,1′-biphenyl (CBP) and using a dopant concentration of 10%. The result for OLED device performance shows the maximum power efficiency (PE) of 45.9 lm W^{-1} and current efficiency (CE) 58.5 cd A^{-1}, while the maximum EQE is 18.2%. However, the turn-on voltage is high enough, is around +3.1 V at 1 cd m^{-2}, and the maximum luminance (L_{max}) of 18,290 cd m^{-2}.[26]

In 2017, Liu *et al*. also synthesized iridium(III)-based yellow phosphorescent dopant. The OLED device's performance shows a very high power efficiency of 69.7 lm W^{-1}, a current efficiency of 85.1 cd A^{-1}, and an EQE of 28.1%. But, the maximum luminance is very low, around

14,940 cd m^{-2} at a voltage of +23.6 V, and has a high driving voltage of around +3.6V.[31] Based on this reason, the presence of a new yellow phosphorescent dopant with high electroluminescence performance, high luminance, and low driving voltage is needed.

Other than yellow OLED, the red OLED is also very useful in VLC applications, especially in taillight cars and red traffic lights. An alternative advantage of modification a structure of phosphorescent dopant is easy for color tuning. Different from yellow phosphorescent dopants, many red phosphorescent dopants easy chosen in the commercial market. The type of red dopant that is easy to find in the market is tris(2-phenylpyridine) iridium(III) ($Ir(ppy)_3$),[18,32] tris[1-phenylisoquinolinato-C2N]iridium(III) ($Ir(piq)_3$),[33,34] etc. Nevertheless, in recent years many researchers still tried to synthesize a new iridium-based red phosphorescent dopant for achieving the highest electroluminescence (EL) performance.[19,35,36] In 2020, Ding *et al.* synthesized saturated iridium-based red phosphorescent containing phenylquinoline ligands. The best EL performance is high luminance of 12,695 cd m^{-2} and high EQE of 14.96% in peak wavelength around 620 nm.[36]

In this study, the utilization of the exciplex system as a co-host for novel phosphorescent dopants has been studied. The exciplex system is optimized by choosing two kinds of donor material (BCzPh and TCTA) blended with two types of acceptor material (CN-T2T and B3PYMPM). The novel phosphorescent dopants (Y1, R1, and R2) were synthesized at Tamkang University, Taiwan. The dopants are optimized by choosing a dopant concentration of 4% and 8%. The differences phenomenon of each structure were detailly explored by EL performance characterization, photoluminescence measurement, impedance spectroscopy, and transient EL response measurement.

1.2 Objectives

The phosphorescent dopant in OLED attracts many researchers due to its superior ability for harvesting singlet and triplet exciton. Implementation of high-performance phosphorescent OLED needed optimization of various hosts. The idea of this study are:

1. Optimization the exciplex-based host by mixing some of the various donor and acceptor materials, also the concentration of dopant.
2. Analyze the device performance of each exciplex host with the current density-voltage-luminescence (JVL) plot, current efficiency-power efficiency, and EQE performance.
3. Study the photophysical phenomenon inside of each host by implementing the photoluminescence measurement.
4. Apply the electrical measurement to explain the differences of capacitance-voltage (CV), Impedance cole-cole, and transient electroluminescence response of each exciplex host.

1.3 Outline

The schematic of this thesis is divided into five parts to make it effortless in understanding, such as:

Chapter 1 Introduction

This chapter will explain the background and overview of OLED works.

Chapter 2 Literature Review.

The literature review is explained here to strengthen the background of this works. The principle of OLED, device parameter, device mechanism, and the principle of each measurement will be described in detail in this chapter.

Chapter 3 Experimental Procedure

The steps of the experimental procedure, the material is used, and the measurement setup will be described in this chapter.

Chapter 4 Result and Discussion

The result of all measurements was plotted and analyzed in detail in this chapter. The phenomenon of each structure will be described in this chapter also.

Chapter 5 Conclusion

The end of this work is summarized clearly in this chapter. The suggestion and the future plan for this work also will be written in this part.

Chapter 2 Literature Review

2.1 Organic Light Emitting Diode

In principle, organic light-emitting diode (OLED) is similar to semiconductor light-emitting diode (LED), the differences are only the constituent material. OLEDs use an organic material made of hydrocarbon chains, while LEDs use an inorganic material.[37] The operational concept of OLED is under applied bias, the holes and electrons were injected from electrodes, and there will be transferred to the emission layer and recombined to emit light. Several advantages in OLED application are high color brightness, lightweight, low power consumption, low operating voltage, fast response, flexibility, and color uniformity.[2,3,5] Because of that, many applications are used OLED as a light source, such as display technology, medical application, solid-state lightning, visible light communication.

Since the first report about organic electroluminescence material in 1963, by Pope *et al.*[38] The single crystal anthracene was inspected under applied bias with very high voltage for more than 400 V. This report makes a breakthrough in OLED development. Although in practical application this invention is not ideal, due to high voltage is required, but it is already a big step at that time. In 1987, Tang *et al.* successfully produced the first practical OLED.[1] The improvement of this device is by decreasing the applied bias becomes DC voltage below +10 V. The OLED structure is using a double organic layer consisting of diamine and Alq_3. The OLED configuration structure is shown in Figure 2.1. Diamine in this structure acts as a hole transport layer (HTL), Alq_3 acts as an electron transport layer (ETL), and both of those materials are connected with anode and cathode, respectively. The external quantum efficiency of this device can achive 1%

with the peak wavelength around 550 nm. On development, this works becomes a basic principle of modern OLED application.

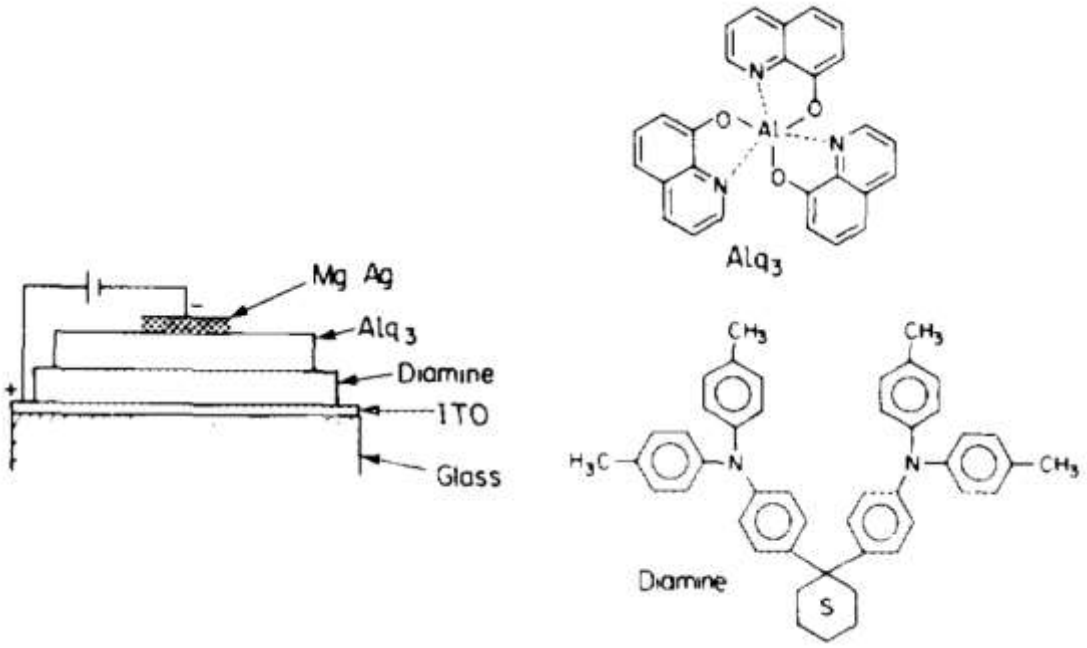

Figure 2.1 First practical OLED by Tang *et al.*[1]

2.1.1 Basic Structure and Principle of OLED

There are two types of energy states in organic material, that is the highest occupied molecular orbital (HOMO) and the lowest unoccupied molecular orbital (LUMO).[37] In the equilibrium states, the electron will occupy the HOMO states. When the electron is excited, the electron will be promoted to higher-level states and occupy the LUMO states. The HOMO and LUMO in organic materials can be illustrated as ground states and excited states in semiconducting materials, in some respects. The excitation of electrons in organic material can happen due to optically or electrically treatment. After the electrons are excited, the electrons will relax back to their original states and produce energy radiatively (light emission) and nonradiative (such as vibrational and rotational state transition).

The basic concept of emission light from OLED is because of the recombination of electrons and holes that are injected from the electrodes.

The recombination of electrons and holes in OLED will generate an exciton. The process of exciton formation starts when the pairs of electrons from the ground states get excitation. The electrons in the ground states consist of two electrons with different spin states, upward and downward spin. The excitation will make 25 % of electron pairs have the same direction as before and called singlet exciton (S1). The 75% of electron pairs will reverse the spin and become triplet exciton (T1) through intersystem crossing (ISC).[39,40] The singlet (S1) and triplet (T1) spin direction is shown in Figure 2.2.

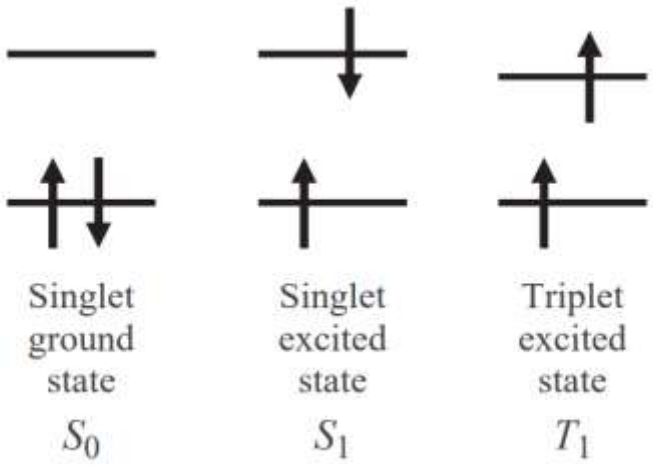

Figure 2.2 Spin configuration in ground states and excited states.[37]

The electron won't stay forever in the excited states. In some time, the electrons will relax back to the ground state and release energy. Depending on the spin, 25% of excited electrons in singlet states will be falling back to ground states and emit a light called fluorescence emission. Whereas, 75% of excited electrons will be transferred to triplet states through the ISC system and will relax back to ground states and emit a phosphorescence emission. The emission mechanism of fluorescence and phosphorescence light by the Jablonski diagram is shown in Figure 2.3.

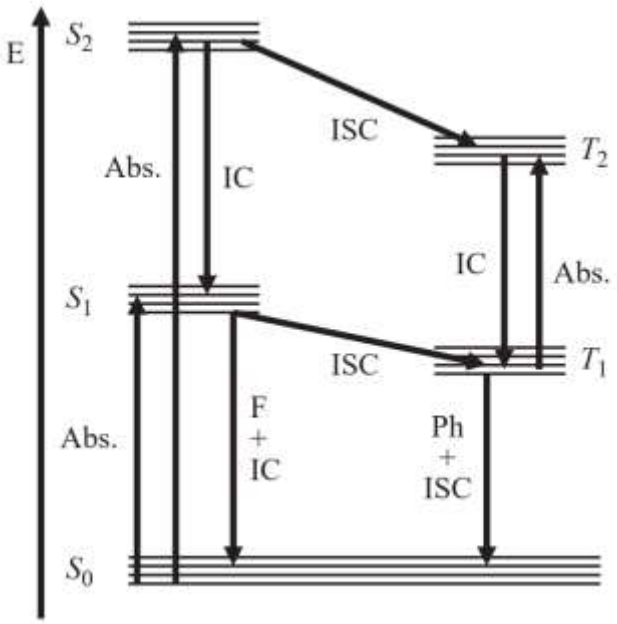

Figure 2.3 The emission mechanism by Jablonski diagram. (IC, internal conversion; ISC, intersystem crossing; Abs., absorption; Ph, phosphorescence; F, fluorescence).[37]

The electrons and holes flow mechanism in OLED devices are concluded in the following steps:

1. Charge injection

   Charge injection in OLED occurs when the electric current is injected into the devices. The carrier will be transferred from metal to organic materials. In a common OLED device, the holes are injected from the anode side to the HOMO level of organic material, while the electrons are injected from the cathode side to the LUMO level of the organic materials. The charge injection mechanism can be caused into two, which are Richardson–Schottky thermionic emission and Fowler–Nordheim (FN) tunneling injection.[37] The illustration of charge injection is shown in Figure 2.4(a). Many researchers were tried reducing the energy barrier between the metal and organic material to realize a low driving voltage.

2. Charge transportation

   After the charge injection, the charge will transport through organic material by the hopping mechanism. The electron will move on the LUMO level of organic materials, and the holes will shift on the HOMO level of organic materials. The local electron and holes concentration will infect the flow of the carrier in organic materials. The carrier flow starts from high carrier concentration to low carrier concentration. The charge transportation mechanism is shown in Figure 2.4(b).

3. Charge recombination

   In the charge recombination mechanism, the electron from the LUMO states with the hole from the HOMO states will generate an exciton. The electron-hole pairs will be realizing energy between radiatively or non-radiatively. The decay of radiative energy will be resulting in an emission of light, while the non-radiative energy decay will be heat generation. The emission from the exciton can be fluorescence and phosphorescence emission depend on the spin direction. The charge recombination mechanism in OLED is shown in Figure 2.4(c).

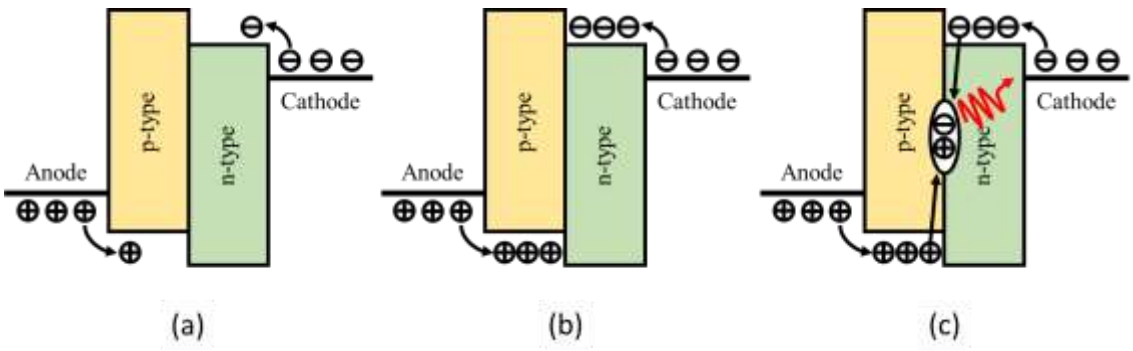

Figure 2.4 Electron and holes flow mechanishm in OLED: (a) charge injection, (b) charge transportation, (c) charge recombination.

In the evolution of OLED structure, the first structure was a single-layer OLED was introduced by Pope *et al.* in 1963.[38] This structure contains a single organic material with two electrode layers. The next innovation of OLED structure was shown by Tang *et al.*[1] Tang was purposed a double-layer OLED which is comprised of p-type and n-type organic materials. The further development that is still used in the OLED structure is multi-layer OLED. Nowadays, most researchers use this type of structure due to the many benefits inside. The structure of multi-layer OLED is shown in Figure 2.5.

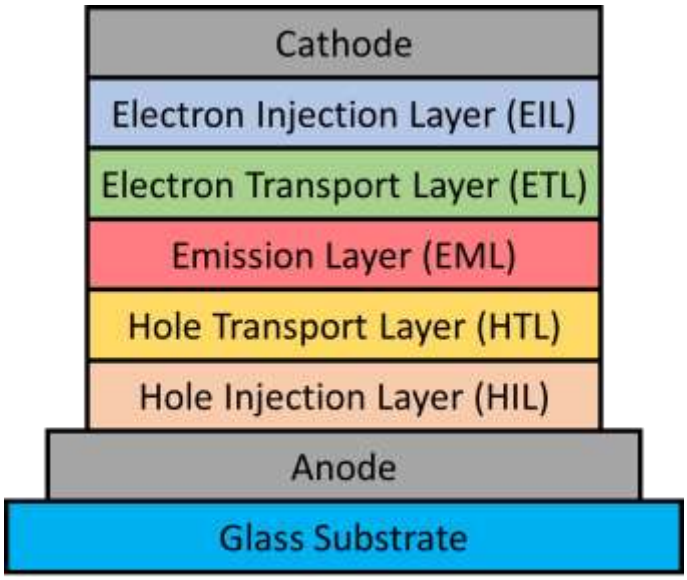

Figure 2.5 The structure of multi-layer OLED.

The function of each organic material in multi-layer OLED was:

1. Hole injection layer (HIL)

   The HIL layer's purpose is to reduce the energy barrier between metal and organic materials. The requirement of this layer is the HOMO level of this material is between the work function of the meral and the HOMO level of the organic materials.

2. Hole transport layer (HTL)

   The HTL layer's function is for helping the electron transportation in the organic materials. The HTL layers need organic materials which have high hole mobility. Another function of the HTL layer is for blocking the electron flow. So, the HTL layer also needed the LUMO level as low as possible.

3. Emission layer (EML)

   The function of this layer is the place of recombination occurs. The electrons from ETL and the holes from HTL will be transferred to EML and form an exciton. The EML layer can be contained a single host material or be mixed with the dopant material. The dopant helps the device to reach higher EL performance. Besides that, the dopant can arrange the wavelength emission of OLED devices.

4. Electron transport layer (ETL)

   This layer function is to help the electron flow from the EIL layer to the EML layer. The requirement of ETL layers is having high electron mobility. In addition, the ETL also helps OLED to block a hole mobilization. The ETL layer also needed the HOMO level as high as possible.

5. Electron injection layer (EIL)

   The function of this layer is to compress the energy barrier for electron injection into OLED devices. The requirement of the EIL layer is the LUMO level of this material is between the work function of the meral and the LUMO level of the organic materials.

2.1.2 Exciplex Formation

An alternative to extracting singlet and triplet exciton is using an exciplex system. If the energy difference between singlet and triplet states is small enough (ΔE_{ST} = 0 - 0.5 eV), the triplet exciton can be up-convert into singlet exciton through reverse intersystem crossing (RISC) by the thermal energy. The emission of this system produces a delayed fluorescence emission and is called thermally activated delayed fluorescence (TADF).[11]

The exciplex (excited complex) system is formed by charge transfer between two different molecules. The exciplex formation system can be made up of molecule manipulation with sophisticated molecular structures. The exciplex also can be formed by physically blending a donor material and acceptor material that involve intermolecular charge transfer. The exciplex-based OLED has the potential to achieve a theoretically 100% IQE. The emission process of the exciplex system is shown in Figure 2.6. The molecule M is denoted as a donor molecule and the molecule Q can be called an acceptor molecule.

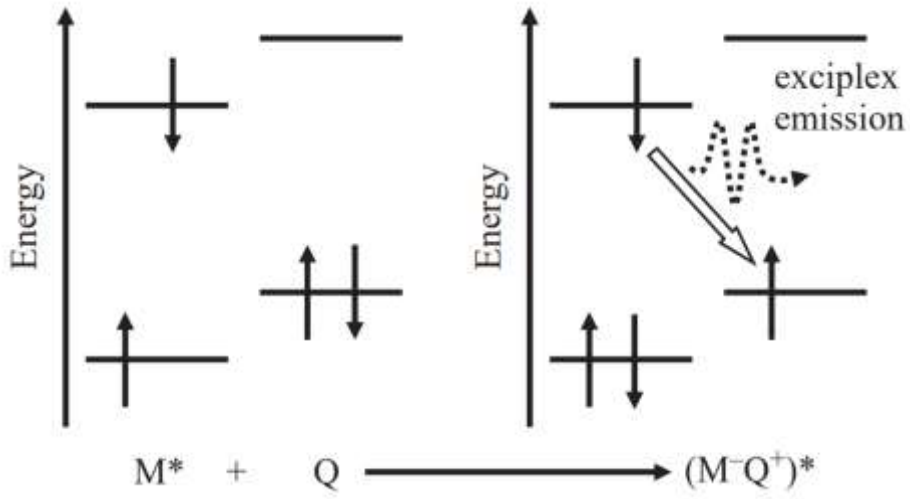

Figure 2.6 The emission process of the exciplex formation system.[37]

Based on the evolution, exciplex formation can be separated into two methods; interfacial system and bulk system.[41] The differences of interfacial system and bulk system can be shown in Figure 2.7(a) and Figure 2.7(b), respectively. The interfacial system can be made by deposition a thin film of a bilayer structure of donor and acceptor organic materials. The recombination area in the interfacial system lies on the interface layer of donor and acceptor materials.

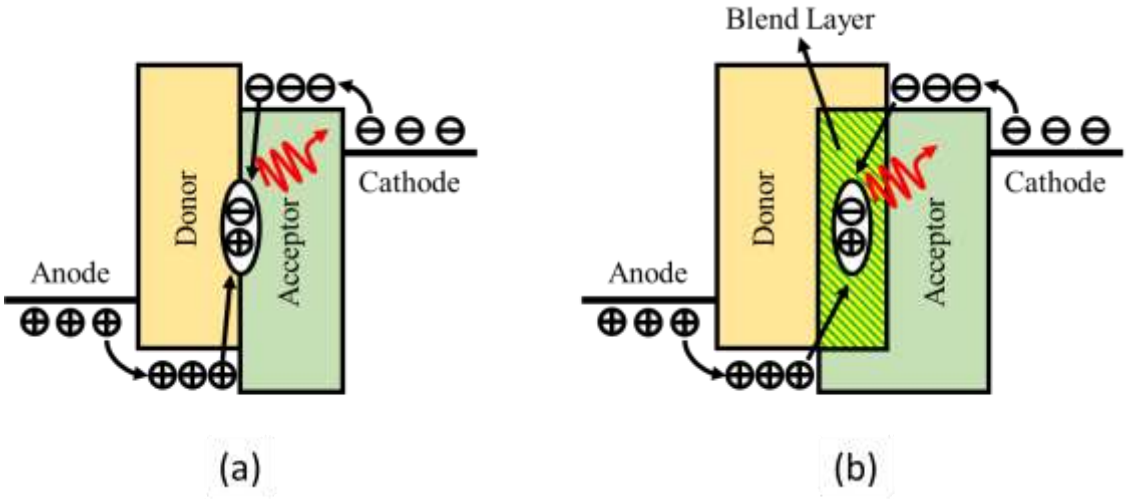

Figure 2.7 The exciplex system (a) interfacial system, (b) bulk system.

Another exciplex formation method is using bulk exciplex. The bulk exciplex system was from blending donor and acceptor material becomes one layer. The purpose of the bulk exciplex system is to increase the recombination area of the emission layer. The recombination area of bulk exciplex is built from each interface of one donor molecule and one acceptor molecule. In 2020, Amin *et al.* studied the interfacial exciplex and bulk exciplex based on a photophysical and electrical characterization. They choose a 9,9'-Diphenyl-9H,9'H-3,3'-bicarbazole (BCzPh) as a donor material and 3′,3‴,3⁗-(1,3,5-triazine-2,4,6-triyl)tris(([1,1′-biphenyl]-3-carbonitrile)) (CN-T2T) as an acceptor material and forming a green exciplex OLED.[41] The bulk exciplex system shows superior performance

compared to the interfacial system. The EQE of the bulk exciplex system was 26.4%, while the interfacial system was 7.7%. This result is becoming a reason for the writer to use a bulk exciplex system for the works.

2.1.3 Exciplex Forming Co-host for Phosphorescent Dopant

The emission of the exciplex system is from the intermolecular charge transfer (ICT) character. However, the wide-emission spectrum of the exciplex system makes the color purity is not very well. The exciplex system has a high EL efficiency, good charge balances, efficient charge injection, and low driving voltage. The utilization of phosphorescent dopants can help OLED for selecting a pure color emission with narrow-spectrum emission. The exciplex system is very suitable as a host for highly effective fluorescent or phosphorescent OLED due to the possibility of extraction triplet exciton.[11] In the exciplex forming co-host for phosphorescent dopant, the exciton is from the host only, not from the dopant. The parameter that needs to consider in the exciplex host for phosphorescent OLED is the efficiency of energy transfer from the exciplex to the dopant. The exciplex forming co-host for phosphorescent dopants mechanism is shown in Figure 2.8.

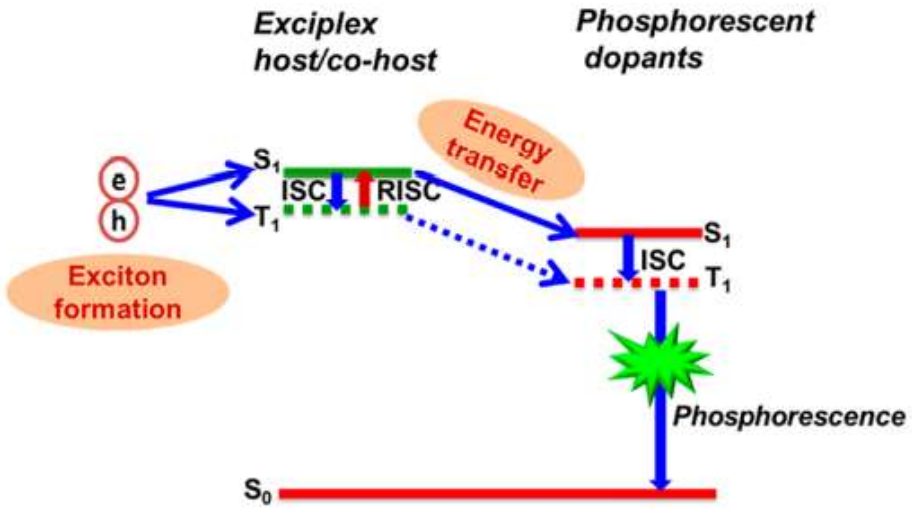

Figure 2.8 The exciplex system as a co-host for phosphorescent dopant.[11]

The singlet energy transfer of exciplex excitons to phosphorescent dopants is known as Förster resonance energy transfer (FRET), while the triplet energy transfer is known as Dexter energy transfer. As the case in Figure 2.8, the emission spectrum of the OLED devices won't be overlap with the emission spectrum from the exciplex host because of the lower triplet states of the dopant than the exciplex host.

2.2 Photoluminescence Measurement

Luminescence is a radiative emission from a certain substance. Luminescence is different from the reflection, refraction, and scattering process. Luminescence occurs due to the electron excitation process.[42] Based on the radiative processes, photoluminescence (PL) is caused by the photoexcitation process. PL measurement is used to analyze materials science and solid-state physics and technology, such as fluorescence and phosphorescence materials. The experimental setup for static PL measurement was shown in Figure 2.9. In Figure 2.9, the C1 is an optical chopper at the normal position, the C2 is an optical chopper for PL decay measurement, the BPF is a band-pass filter, the LPF is a long-pass filter, the NDF is a neutral density filter, and the PC is a personal computer.

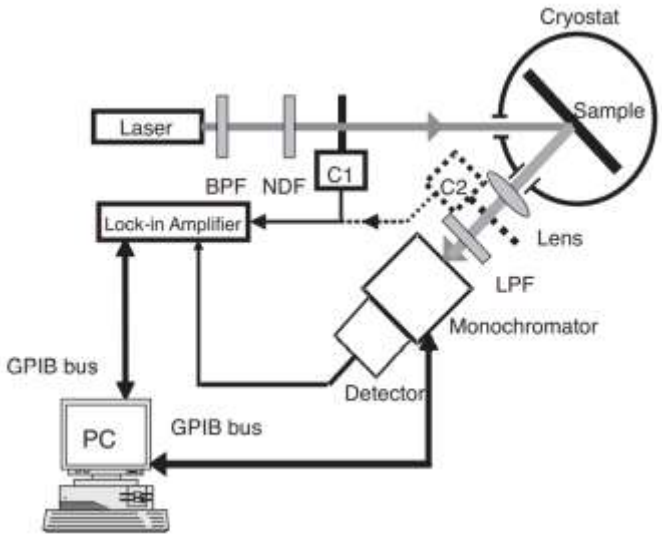

Figure 2.9 The experimental setup of PL measurement.[42]

PL measurement is included in the quantum mechanical process where the photon will transfer energy to the electron in ground states, and the electron will excite into an excited state within only femtosecond time.[42] The result of PL measurement can be emission spectra (PL spectra) or time-resolved photoluminescence (TRPL) plots. In the OLED research field, the PL spectra are used to detect the emission spectrum for each emitting material (single or exciplex materials, fluorescence or phosphorescence materials, etc.).[15–17] In addition, the PL spectra can be used to analyze a degradation mechanism for emitting materials.[15] The TRPL results are used to see the TADF phenomenon in the exciplex host system and the energy transfer quality from a host to a dopant system.[16] The examples of PL spectra and TRPL results are shown in Figure 2.10(a) and Figure 2.10(b), respectively.

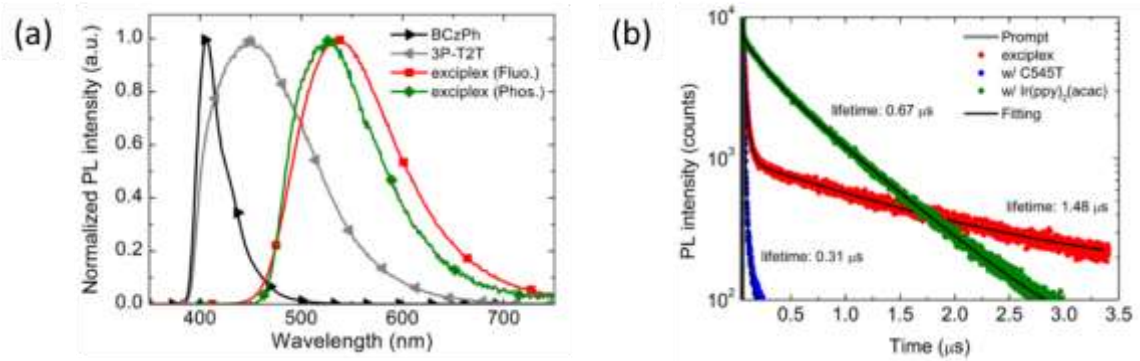

Figure 2.10 The PL measurement; (a) PL spectra, (b) TRPL.[16]

2.3 Impedance Spectroscopy Measurement

Impedance spectroscopy (IS) has a function to analyze the electrical characterization of organic material in OLED devices. In the research field, IS measurements were used to study dynamics charge mobilization,[43,44] OLED degradation mechanism,[45] resistance values in AC circuit,[46] electrical properties of materials.[47] Impedance spectroscopy will be resulting in the real-impedance (Z') value and imaginary impedance (Z")

value of organic materials. Every OLED device can be illustrated as an equivalent electronic circuit of the device. The impedance result will be plotted as an impedance cole-cole plot (Z-plot) and will be fitted to get an equivalent circuit of the OLED devices. In the IS measurements, the data was served in two ways, capacitance-voltage (CV) plot and impedance cole-cole plot (Z-plot). Each data type will be explained more in the next subchapter.

2.3.1 Capacitance-Voltage Plot

In this study, we plot the impedance data measurement with a capacitance-voltage (CV) plot model. This plot model can help us to analyze the charge injection behavior of OLED devices.

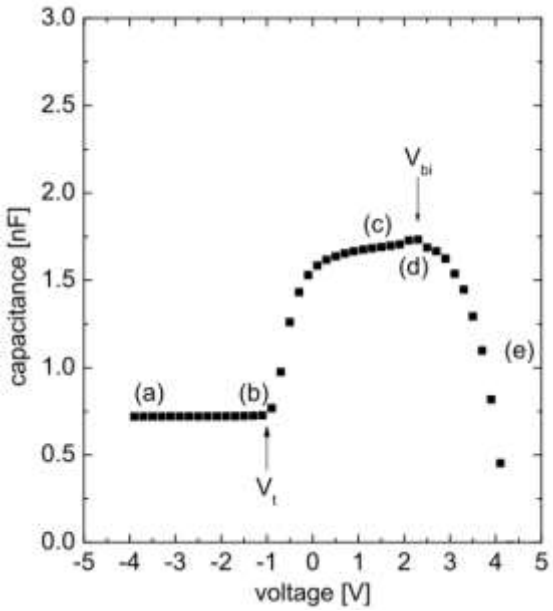

Figure 2.11 The capacitance-voltage (CV).[43]

Nowy *et al.* explained the charge carrier of OLED devices using a CV plot.[43] The complex impedance (Z' and Z") can be converted to capacitance value with this relation:

$$C = \frac{dQ}{dV} = \frac{1}{2\pi f}\ x\ \frac{-Z''}{(Z')^2 + (Z'')^2} \qquad (1)$$

The capacitance-voltage plot from impedance measurements was shown in Figure 2.11. The illustration of electrons and holes movement under different applied bias as shown in Figure 2.12, helps us to analyze a capacitance-voltage plot from impedance measurement. As shown the Figure 2.11, the capacitance response under applied bias is divided into five region, which are:

(a) Without charge injection ($V_0 < V_t$)

The first region occurs when the bias voltage (V_0) is under the threshold voltage (V_t). No charge injection from electrodes to the organic layers. These region can be illustrated as shown in Figure 2.12(a). The high injection barrier at metal and organic materials causes not enough energy from carriers to inject through materials.

(b) The carrier start to inject from electrodes ($V_0 = V_t$)

This region occurs when the bias voltage (V_0) was passed the threshold voltage (V_t). These region can be illustrated as shown in Figure 2.12(b). The capacitance value of the OLED device starts to increase along with increasing the applied bias.

(c) The charge accumulated in OLED ($V_t < V_0 < V_{bi}$)

After the bias voltage (V_0) is higher than a threshold voltage (V_t), more charge will be accumulated in the organic materials until the V_0 achieves the built-in voltage (V_{bi}) from OLED, as shown in Figure 2.12(c).

(d) The charge recombination started ($V_0 = V_{bi}$)

This region occurs when the bias voltage (V_0) is the same as the built-in voltage (V_{bi}). The charge accumulation will be stopped, and the charge recombination will be started soon. The electron injection

will be started from the cathode side, as shown in Figure 2.12(d). The capacitance value of the OLED device at this part is the maximum value.

(e) The charge annihilated ($V_0 > V_{bi}$)

This region occurs when the bias voltage (V_0) is higher than the built-in voltage (V_{bi}). The electrons and holes will be recombined and generate light, as shown in Figure 2.12(e). The charge inside the OLED will be annihilated, which is indicated by a decrease in the value of the capacitance.

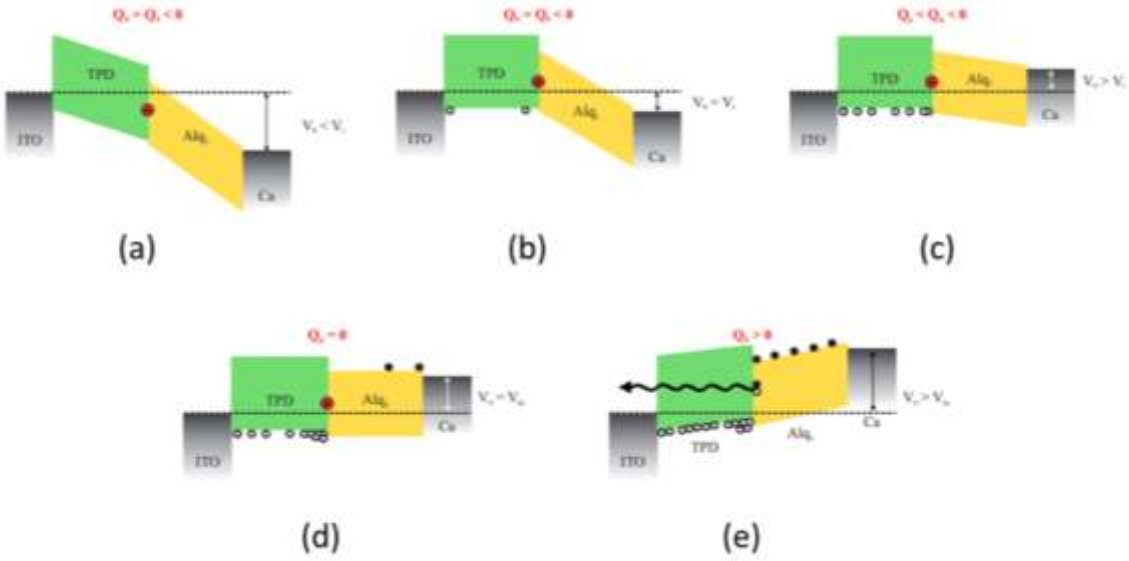

Figure 2.12 The illustration of simplified band diagram OLED under applied bias; (a)$V_0 < V_t$, (b) $V_0 = V_t$, (c) $V_t < V_0 < V_{bi}$, (d) $V_0 = V_{bi}$, (e) $V_0 > V_{bi}$ [43]

2.3.2 Impedance Cole-cole (Z-Plot)

This impedance cole-cole plot method was applied to extracting RC equivalent circuits of OLED devices. The example of impedance cole-cole plots is shown in Figure 2.13.

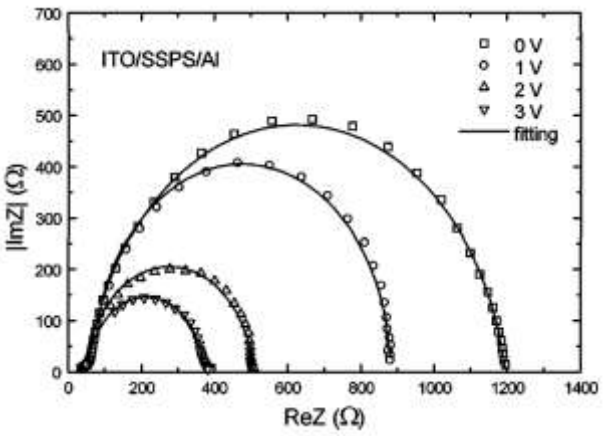

Figure 2.13 The example of impedance cole-cole plots.[48]

Impedance (Z) cole-cole plot can be obtained by giving a fixed applied bias into the OLED devices and then sweeping the frequency from high to low frequency. The minimum values of the real-impedance (Z') was the impedance values at high frequency, and it can be represented as sheet resistance in OLED devices. On another side, the maximum real-impedance value (Z'') can be defined as the sum of series and parallel resistance (R) and capacitance (C).[48]

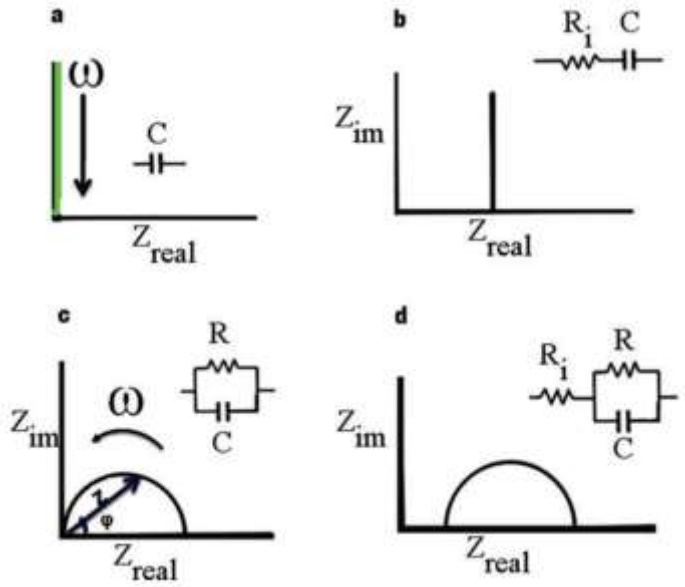

Figure 2.14 The component response of; (a) capacitor, (b) resistor series with capacitor, (c) resistor parallel with capacitor, (d) resistor in series with parallel RC.[49]

The equivalent circuits for OLED devices were built from capacitor and resistor components. So, each component response that influences the impedance cole-cole plot was needed to be learned. The capacitor and resistor response to the impedance plots is shown in Figure 2.14. The equivalent circuits of OLED devices chosen by the author are shown in Figure 2.15. The equivalent circuits are constructed by the series connection of two parallel RC components and a single resistor component. Chen *et al.* selected this equivalent circuits model because of the OLED device containing two regions with differential electrical behavior (p-type and n-type).[50]

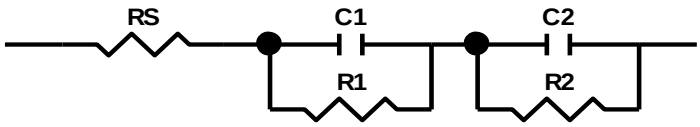

Figure 2.15 The equivalent circuits of multi-layer OLED.

The sheet resistance (R_s) can be described as a internal resistance between two metal layer in semiconductor devices. Han *et al.* described the first RC parallel in the equivalent circuits are representative of one electrical behavior, which is hole conduction behavior (p-type materials). Then, the next RC parallel is considered as an electron conduction behavior (n-type materials).[51]

2.4 Transient Electroluminescene Measurement

The transient electroluminescence (TREL) measurement was a good approach to study recombination characteristics,[52] carrier mobility, charge injection and transportation.[53,54] To do TREL measurements, a short voltage pulse was given to the OLEDs, and the EL response of the devices were captured and analyzed. The voltage pulse characteristic and

TREL measurement response of OLED devices is shown in Figure 2.16. The response of the TREL measurement can be divided into three parts; the time delay part, the rising part, and the decay part.

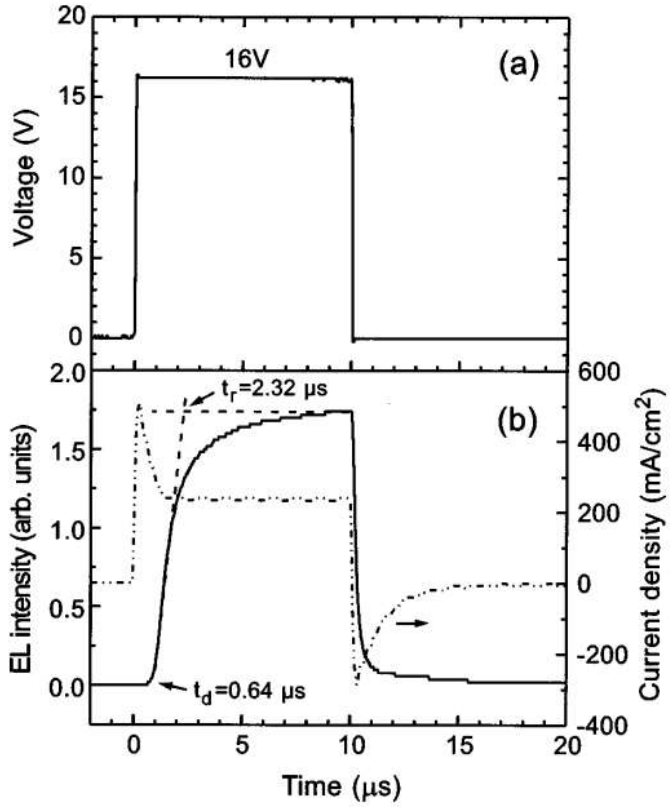

Figure 2.16 The voltage pulse characteristic and TREL measurement response of OLED devices.[55]

Chapter 3 Experimental Procedure

3.1 OLEDs Structure

This study focused on the optimization of exciplex hosts for phosphorescent OLEDs. The variation of exciplex hosts consists of two donor materials 9,9'-Diphenyl-9H,9'H-3,3'-bicarbazole (BCzPh), 4,4',4''-Tris(carbazol-9-yl)triphenylamine (TCTA), and two acceptor materials 3′,3‴,3′′′′-(1,3,5-triazine-2,4,6-triyl)tris(([1,1′-biphenyl]-3-carbonitrile)) (CN-T2T), 4,6-Bis(3,5-di(pyridin-3-yl)phenyl)-2-methylpyrimidine, 4,6-Bis(3,5-di-3-pyridinylphenyl)-2-methylpyrimidine (B3PYMPM). The exciplex hosts (donor and acceptor) were mixed by bulk exciplex with the ratio of 1:1 and thickness of 30 nm. The phosphorescent dopants as a guest in OLEDs structure fabricated in Tamkang University, Taiwan. There are three Iridium (Ir) based phosphorescent dopants which are one yellow dopant (Y1) and two red dopants (R1 and R2). The dopant concentration is using in this study are 4% and 8%.

Table 3.1 Device configuration of BCzPh donor material.

<table>
<tr><th>Anode</th><th>HIL</th><th>HTL1</th><th>HTL2</th><th>EML</th><th>ETL</th><th>EIL</th><th>Cathode</th></tr>
<tr><td rowspan="5">LT-ITO
(150 nm)</td><td rowspan="5">HATCN
(30 nm)</td><td rowspan="5">TAPC
(60 nm)</td><td rowspan="5">BCzPh
(10 nm)</td><td>BCzPh
:CN-T2T:X
(1:1:4%)
(30 nm)</td><td rowspan="2">CN-T2T
(50 nm)</td><td rowspan="5">LiF
(1 nm)</td><td rowspan="5">Al
(120 nm)</td></tr>
<tr><td>BCzPh
:CN-T2T:X
(1:1:8%)
(30 nm)</td></tr>
<tr><td>BCzPh
:B3PYMPM:X
(1:1:4%)
(30 nm)</td><td rowspan="2">B3PYMPM
(50 nm)</td></tr>
<tr><td>BCzPh
:B3PYMPM:X
(1:1:8%)
(30 nm)</td></tr>
</table>

Table 3.2 Device configuration of TCTA donor material.

Anode	HIL	HTL1	HTL2	EML	ETL	EIL	Cathode
LT-ITO (150 nm)	HATCN (30 nm)	TAPC (60 nm)	TCTA (10 nm)	TCTA :CN-T2T:X (1:1:4%) (30 nm)	CN-T2T (50 nm)	LiF (1 nm)	Al (120 nm)
				TCTA :CN-T2T:X (1:1:8%) (30 nm)			
				TCTA :B3PYMPM:X (1:1:4%) (30 nm)	B3PYMPM (50 nm)		
				TCTA :B3PYMPM:X (1:1:8%) (30 nm)			

The purposed device structure for BCzPh donor material was fabricated corresponding to Table 3.1. Moreover, the device structure of TCTA donor material is shown in Table 3.2. The X in the purposed device structure is the phosphorescent dopant (Y1, R1, R2) produced by Tamkang University, Taiwan. These works are focusing on device optimization to find a suitable exciplex host for a new phosphorescent emitter. Several measurements such as device performance, photophysical, and electrical measurements were done to analyze the phenomenon happening inside each structure.

3.2 OLEDs Materials

In this experiment, the energy level of each structure used is shown in Figure 3.1 The exciplex host was tested in this study, which are BCzPh: CN-T2T, BCzPh:B3PYMPM, TCTA:CN-T2T, and TCTA:B3PYMPM. Every exciplex host was mixed with ‘X’ as a phosphorescent emitter. All the materials that used in the OLED structure are described below:

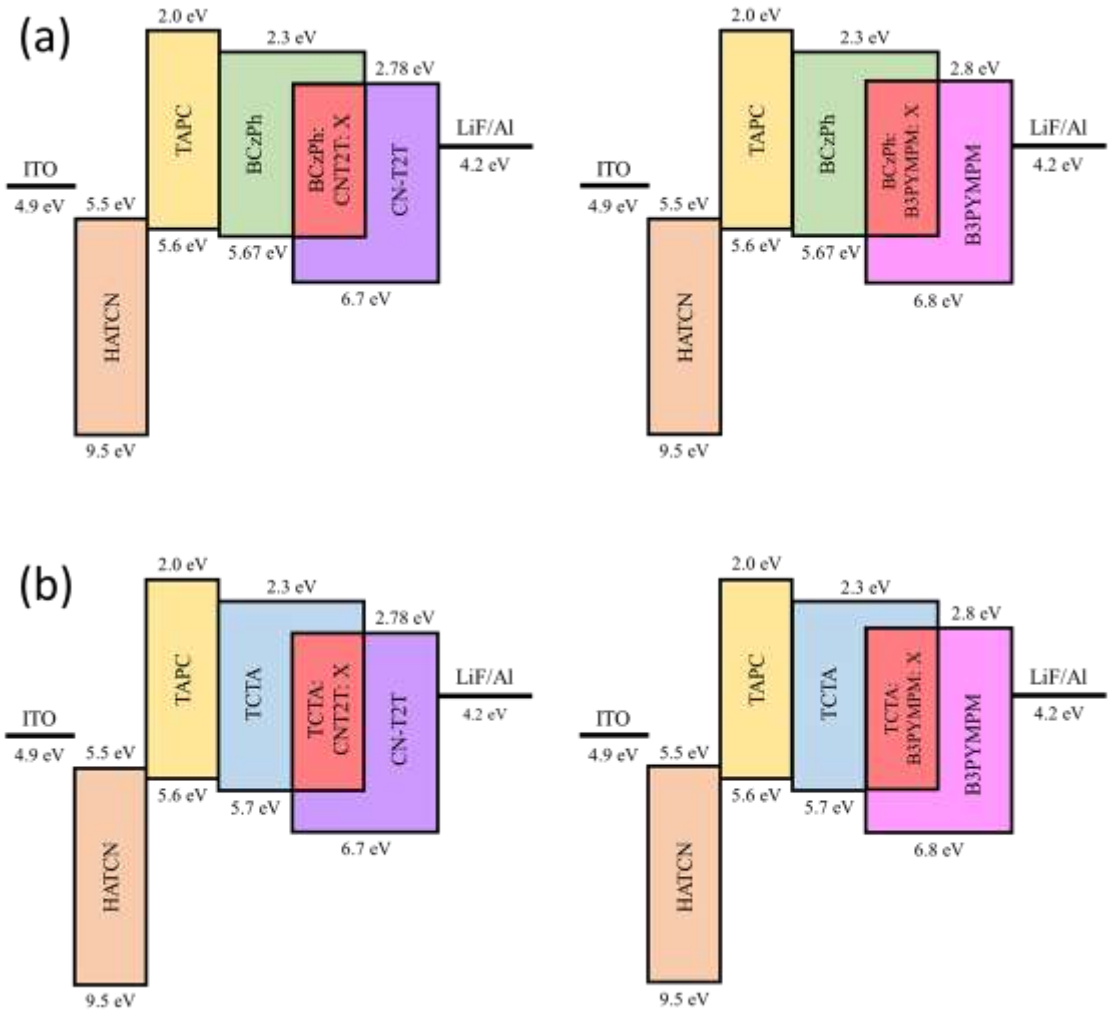

Figure 3.1 Energy level of: (a) BCzPh device, (b) TCTA device.

a) Indium Tin Oxide

Indium tin oxide (ITO) was used as the anode in the OLED structure with a resistance of 15 Ω $\square^{-1}$. The ITO is purchased from Lumtec Corporation and patterned with a laser pattern machine to become the 5 pixels ITO pattern. The pixel area of the ITO pattern is 0.04 cm^2.

b) HATCN

1,4,5,8,9,11-Hexaazatriphenylenehexacarbonitrile or commonly known as a HATCN was purchased from Shine Materials

Technology Co., Ltd. HATCN is used as a hole-injection layer (HIL) in the OLED structure. HATCN can improve the hole carrier injection efficiency that works as an interface between ITO and the hole-transport layer (HTL). The HATCN molecular structure is shown in Figure 3.2.

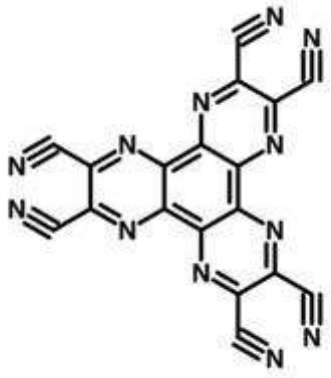

Figure 3.2 The HATCN molecular structure.

c) TAPC

4,4′-Cyclohexylidenebis[N,N-bis(4-methylphenyl)benzenamine] as known as a TAPC was purchased from Shine Materials Technology Co., Ltd. TAPC is used as a hole-transport layer (HTL) with an energy level of HOMO is 5.6 eV and LUMO is 2.0 eV. The TAPC molecular structure is shown in Figure 3.3.

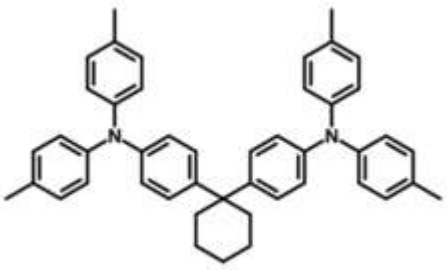

Figure 3.3 The TAPC molecular structure.

d) BCzPh

9,9'-Diphenyl-9H,9'H-3,3'-bicarbazole as known as BCzPh was purchased from Shine Materials Technology Co., Ltd. The BCzPh molecular structure is shown in Figure 3.4. The BCzPh energy level of HOMO is 5.67 eV, and LUMO is 2.3 eV. The exciplex in the emission layer of OLED using BCzPh as an electron donor host material. Besides that, the BCzPh was used as an electron blocking layer to block the electron leakage from the cathode side.

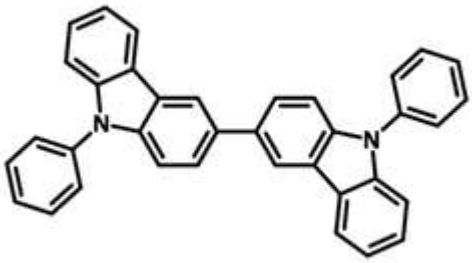

Figure 3.4 The BCzPh molecular structure.

e) TCTA

4,4',4''-Tris(carbazol-9-yl)triphenylamine or commonly known as a TCTA was purchased from Shine Materials Technology Co., Ltd. The TCTA energy level of HOMO is 5.7 eV, and LUMO is 2.3 eV. The TCTA molecular structure is shown in Figure 3.5. The TCTA is used as an electron donor host material in exciplex formation and electron blocking layer in OLED devices.

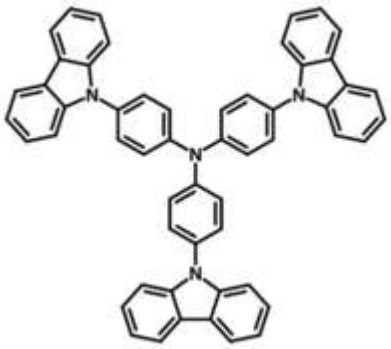

Figure 3.5 The TCTA molecular structure.

f) Iridium (Ir) based phosphorescent dopant

The phosphorescent dopants used in this study were fabricated by Tamkang University, Taiwan. There are three phosphorescent dopants produced, namely: two red dopants (R1 and R2) and one yellow dopant (Y1). The phosphorescent dopants are used as a guest for the host-guest system in exciplex formation. The phosphorescent dopants were fabricated using iridium (Ir). The iridium-based dopant is the best element for phosphorescent dopant types in general.

g) CN-T2T

CN-T2T or 3′,3‴,3⁗-(1,3,5-triazine-2,4,6-triyl)tris(([1,1′-biphenyl]-3-carbonitrile)) was purchased from Shine Materials Technology Co., Ltd. The CN-T2T energy level of HOMO is 6.7 eV, and LUMO is 2.78 eV. The CN-T2T is used as an electron acceptor host material to form an exciplex and used as an electron transport layer (ETL) in OLED devices. The CN-T2T molecular structure is shown in Figure 3.6.

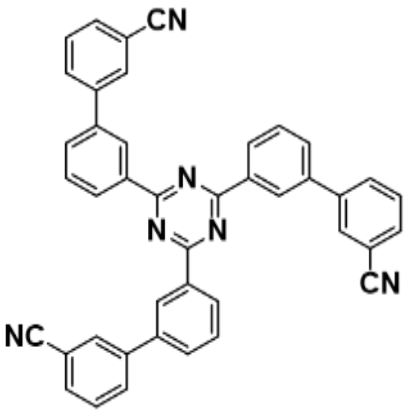

Figure 3.6 The CN-T2T molecular structure.

h) B3PYMPM

4,6-Bis(3,5-di(pyridin-3-yl)phenyl)-2-methylpyrimidine or as known as B3PYMPM was purchased from Shine Materials Technology Co., Ltd. The B3PYMPM molecular structure is shown in Figure 3.7. The B3PYMPM energy level of HOMO is 6.8 eV, and LUMO is 2.8 eV. B3PYMPM used as an electron transport layer (ETL) in the OLED device. On the exciplex side, B3PYMPM acts as an electron acceptor material and mixes with donor material to become a host for phosphorescent dopants.

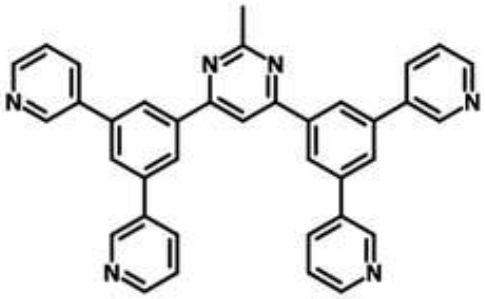

Figure 3.7 The B3PYMPM molecular structure.

3.3 OLEDs Fabrication

The steps of OLED device fabrication are shown in Figure 3.8. The fabrication process consists of substrate preparation, material preparation, material deposition, and device encapsulation. The OLED deposition method in this study uses vacuum deposition for small molecule material. The explanation of each step in OLED fabrication will be explained in more detail in the next sub-chapter.

Figure 3.8 Device fabrication process for the OLEDs device.

3.3.1 Substrate Preparation

The first step for substrate preparation is patterning the ITO glass. The substrate is composed of indium tin oxide (ITO) with the thickness of 150 nm on a glass substrate, and we usually call it ITO-substrate. The ITO-substrate needs to be patterned into 5 pixels before being used for OLED devices.

The big ITO-substrate is cut into the size of 100 × 100 mm and patterned with a laser cutting machine, as shown in Figure 3.9(a). The pattern for 100 × 100 mm ITO-substrate is shown in Figure 3.9(b). After finishing the first step, the ITO substrate needs to be cut into 28 x 18 mm with 5 pixels in each sample. The ITO substrate is ready now and will go to the cleaning process.

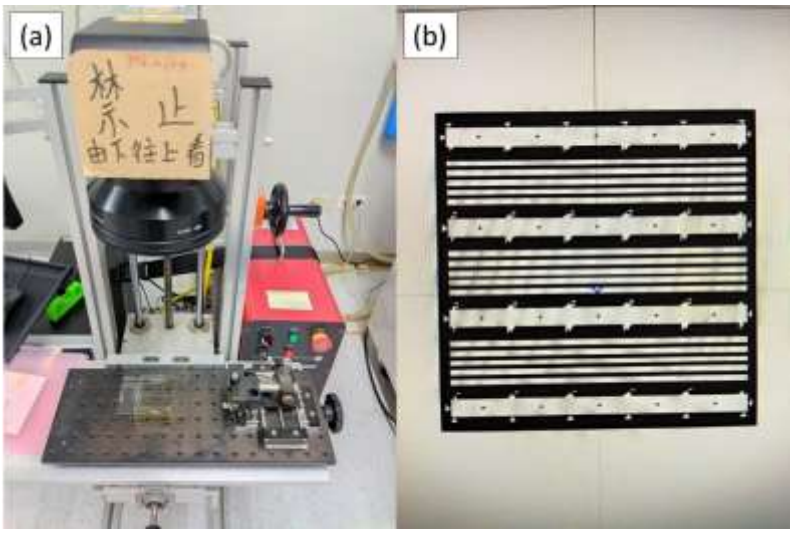

Figure 3.9 Laser cutting machine (a) and 5 pixel ITO-pattern (b).

The cleaning process starts with cleaning the substrate using detergent. Then, the substrate was cleaned using deionized water, acetone, and isopropyl alcohol in the ultrasonic bath for 10 minutes, respectively. The substrate was dried by a nitrogen (N_2) gas blower in the ambient condition. The ultrasonic bath and gas N_2 blower system is shown in Figure 3.10. Next, ITO-substrate is clean now and will use as an anode in OLED devices. Before doing a deposition process, material preparation is necessary. The material preparation will explain more detail in the next chapter.

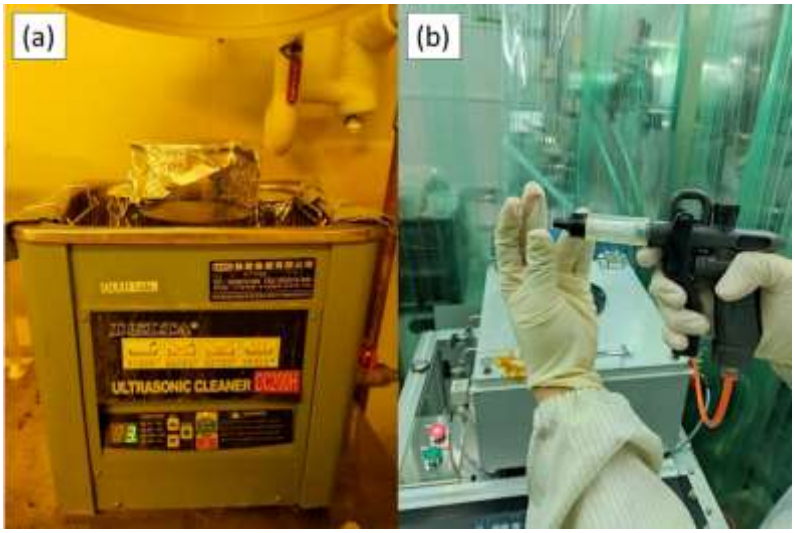

Figure 3.10 Ultrasonic bath (a) and N_2 gas blower (b).

3.3.2 Material Preparation

The material preparation begins with sublimating all the organic material using a vacuum purification system (~5 × 10^{-6} torr) before being used for the deposition process. After the sublimation process, the purified material needs to be placed in a material holder to use in the chamber. There are three types of material holders, that are organic tubes, organic boats, and metal boats, as shown in Figure 3.11.

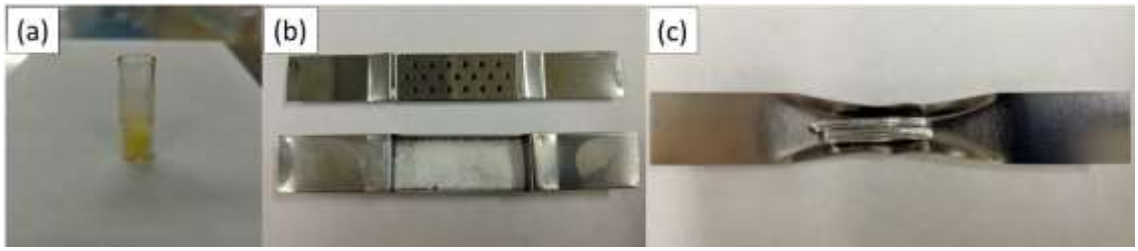

Figure 3.11 Organic tube (a), organic boat (b), and metal boat (c).

All the material used in this study was placed in the thermal evaporation chamber in their respective positions, as shown in Figure 3.12(a). The clean ITO-substrate was placed in the chamber using a holder usually we call an organic mask, as shown in Figure 3.12(b). The thickness sensor and deposition rate sensors in the chamber need to notice with a lifetime of >90% to get an accurate result.

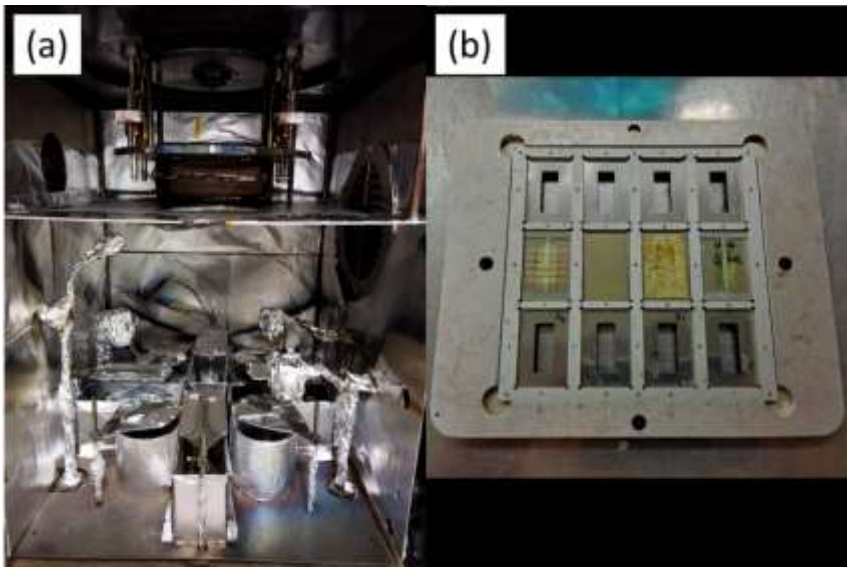

Figure 3.12 Thermal evaporation chamber (a) and organic mask holder (b).

Before starting the deposition process, the chamber needs to vacuum under a high vacuum level of 2×10^{-6} torr. The appropriate thickness of each material used in this study was calibrated by a surface profilometer (Dektak XT) from Bruker, as shown in Figure 3.13. The material preparation is finished, and the samples are ready for the next step. The material deposition process described clearly in the next sub chapter.

Figure 3.13 Surface profilometer (Dektak XT).

3.3.3 Material Deposition

The material deposition process starts from pumping out the chamber into a high-pressure level. There are two kinds of vacuum systems in thermal evaporation systems. First, the pressure needs to be pumped 5×10^{-2} to clean the chamber from dust and pump out the oxygen. After that, the chamber was pumped out until 5×10^{-6} using a high vacuum cryogenic pump. A high vacuum is needed to ensure the environment inside the

chamber is clean and does not disturb the deposition process. The oxygen level inside the chamber needs to be very low because the oxygen can interact with organic material and decay organic material.

To control the material deposition process is using a computer system as shown in Figure 3.14(a). The control center in the thermal evaporation system by using current (A) for each boat. The temperature sensors of each source were displayed in the control box, as shown in Figure 3.14(b). All organic material was needed to preheat under 20~30 A, depending on the materials. Then, the deposition process of each layer can be started from the HIL to EIL with maintaining the rate of each material. The deposition rate for organic material is variated from 0.3~0.5 Å/s. The deposition starts layer by layer until the emission layer (EML), which need three materials to make bulk layer. The sample was rotated with a speed of 8 rpm to maintain the uniformity of each surface layer.

Figure 3.14 Computer system in thermal evaporation system (a) and current controller and temperature sensor display (b).

When depositing the electron injection layer, in this case, LiF, it was recommended to let the material waste around 50 Å to remove the impurity oxide on the surface of LiF. After depositing all organic material, the organic mask needs to change into a cathode mask for aluminum. The cathode mask in this study is shown in Figure 3.15. The last step is the deposition of aluminum as a cathode to contact the OLED. The deposition rate for the aluminum is around 4~5 Å/s. After depositing all the material, the OLED device is required to be encapsulated with ultraviolet (UV) glue and encapsulation glass. The device encapsulation process will explain in the next sub chapter.

Figure 3.15 Cathode mask holder.

3.3.4 Device Encapsulation

After the material deposition process, the OLED device needs to be protected from oxygen exposure. The material holder was moved from the chamber to the glove box without oxygen with a moisture of < 0.1 ppm. The encapsulation glass in this study is using opaque glass. The encapsulation glass was placed in the holder, and the edge of the glass was

covered by UV glue. The holder and the encapsulation glass are shown in Figure 3.16(a). While, the type of UV glue used is EXC345, as shown in Figure 3.16(b).

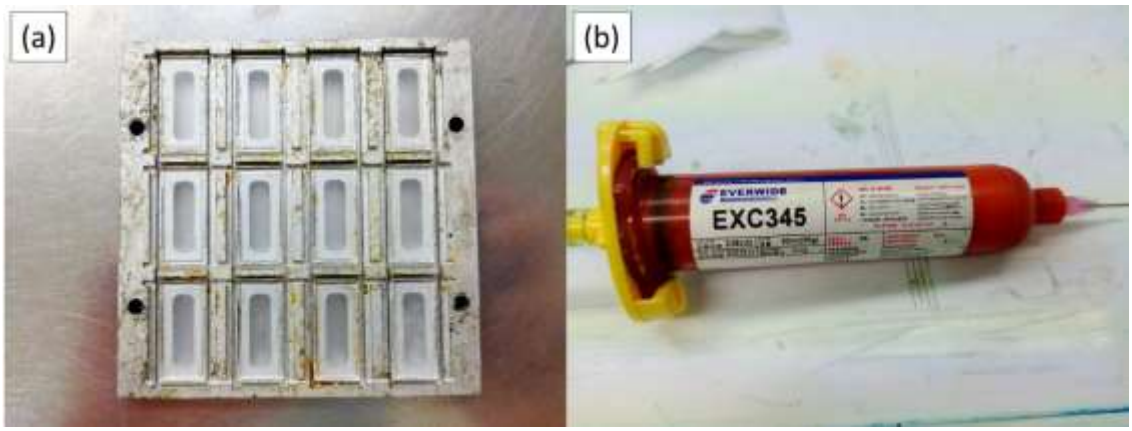

Figure 3.16 Encapsulation glass and holder (a) and UV glue EXC345 (b).

Then, the OLED device was attached to the top of the encapsulation glass. The final device needs to be placed under UV light exposure for around 90~120 seconds. The encapsulation glass aims to protect the organic material inside OLED from oxygen and maintain the vacuum inside the OLED. The final OLED device looks like in Figure 3.17. One OLED device has five pixels with a pixel area size of 0.04 cm^2. After the encapsulation process, the device fabrication process is finished. The OLED devices are ready for the measurement process to analyze the phenomenon inside.

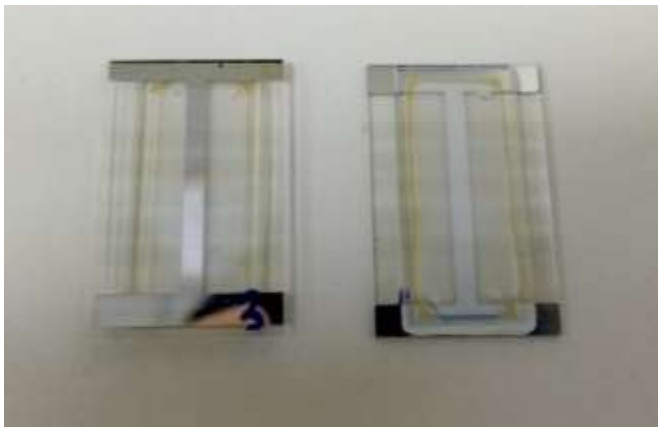

Figure 3.17 Final device of OLED.

3.4 OLEDs Measurement

The OLED measurements have been done consist of device performance characterization, photophysical characterization, and electrical characterization. All of the device measurement was done in our center and will be explained more in detail.

3.4.1 Device Performance Characterization

The device characterization focuses on analyzing the device performance of each structure. The purpose of this study is to optimize the exciplex host structure based on a new phosphorescent emitter. The current density-voltage-luminescence (JVL), power efficiency-current efficiency, external quantum efficiency (EQE), and emission spectra were obtained by spectrophotometer. The device was supplied voltage by source meter. The model of a spectrophotometer and the source meter is used in this study is Photo Research PR-655 and Keithley Instrument Model-2400, as shown in Figure 3.18(a) and Figure 3.18(b), respectively.

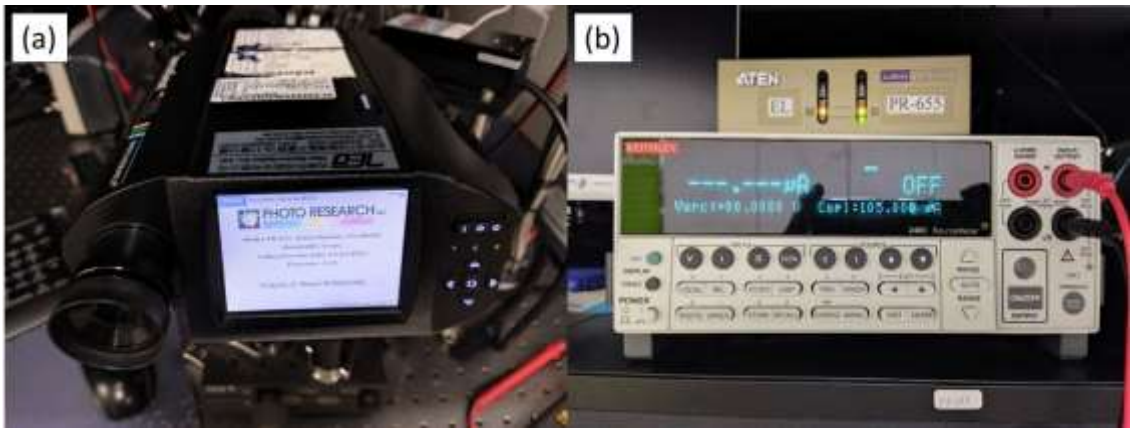

Figure 3.18 Photo Research PR-655 (a) and Keithley Model-2400 (b).

The spectrophotometer, source meter, and computer are integrated into a system. The OLED device was placed on the device holder and turned on all of the systems. The OLED is given a voltage of +3 V to match

the detector spot with the pixels. The device is given a voltage from +0 V to +8 V, and for each step of +0.2 V, the spectrophotometer will catch the light and measure it. All of the data of each structure was taken and plotted with the OriginPro software from OriginLab.

3.4.2 Photophysical Characterization

The photoluminescence (PL) spectrum, photoluminescence quantum yield (PLQY), and time-resolved photoluminescence (TRPL) measurements were accomplished by a spectrofluorometer in our center. The model of the spectrofluorometer is HORIBA Scientific FluoroMax Plus, as shown in Figure 3.19. The sample which used for this measurement is a thin film of material of emission layer. The thin film was made by a thermal evaporation system, which was deposited on the clean quartz glass substrate with the size 1 x 1 cm.

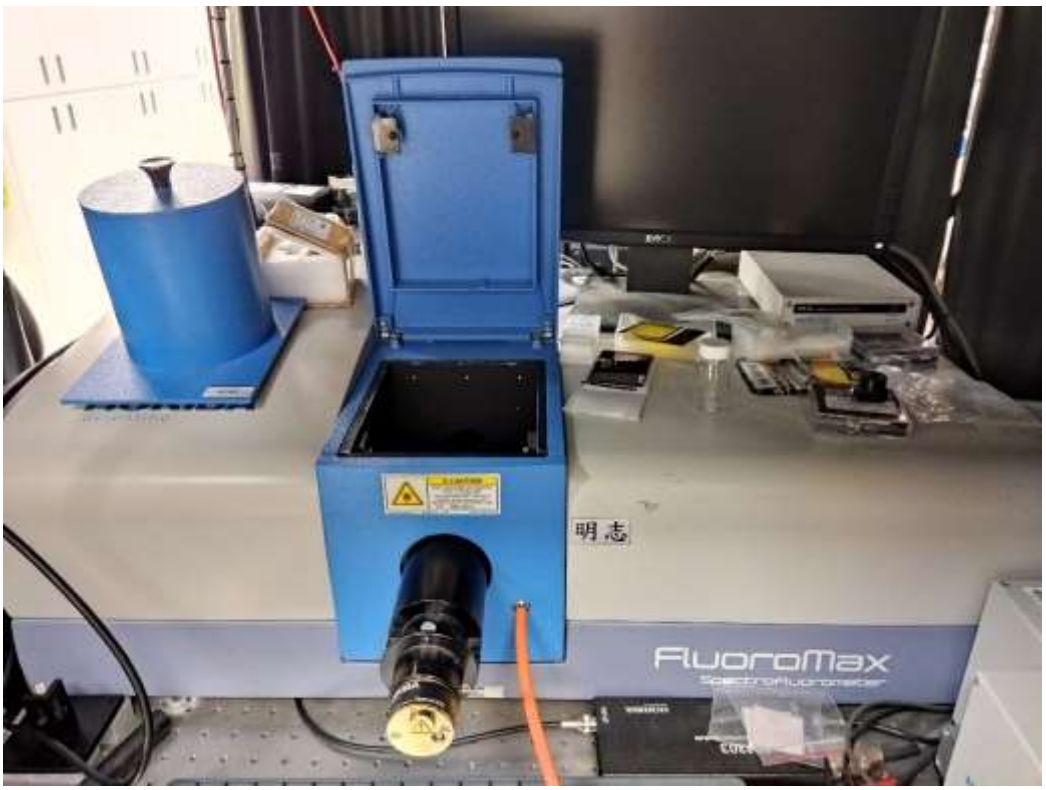

Figure 3.19 HORIBA Scientific FluoroMax Plus.

The PL measurement was assisted by the excitation light ozone-free xenon arc lamp with the wavelength (λ_{ex}) of 305 nm under room temperature. Whereas, TRPL measurement was assisted by NanoLED pulse diode with the wavelength (λ_{ex}) of 320 nm and the frequency of 250 kHz at nitrogen (N_2) ambient conditions. The test sample for PL measurement is the emission material which consists of a single material (BCzPh, TCTA, CN-T2T, and B3PYMPM) and bulk material (BCzPh:CN-T2T, BCzPh:B3PYMPM, TCTA:CN-T2T, TCTA:B3PYMPM) with and without the dopant (Y1, R1, and R2).

3.4.3 Electrical Characterization

The electrical characterization measurement is composed of impedance spectroscopy (IS), capacitance-voltage (CV) measurement, and transient electroluminescence (TREL) measurement. The electrical measurement was measured by integrated system Paios (FLUXiM), as shown in Figure 3.20.

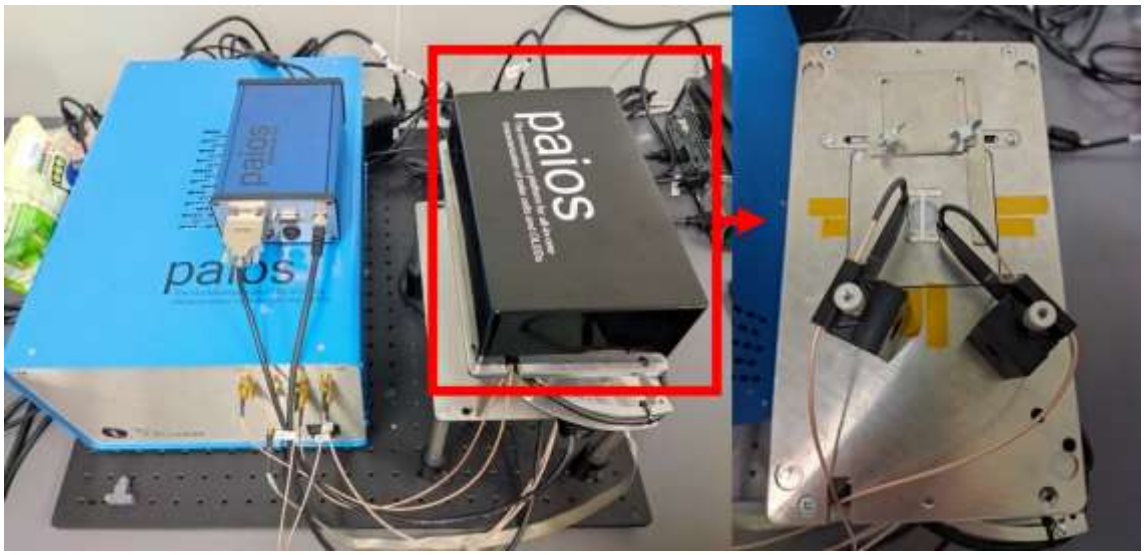

Figure 3.20 Integrated system Paios measurement (FLUXiM).

In impedance spectroscopy, there are two types of measurement setup: voltage sweep and frequency sweep. The voltage sweep testing was done by sweeping the voltage from +0 V to +6 V, with the step of +0.2 V. The frequency used was fixed at 1 kHz, and the low frequency is chosen because the device response is better without the noise. This type of measurement results in a capacitance-voltage (CV) plot. Furthermore, the frequency sweep system is done by sweeping the high frequency of 10 MHz to a low frequency of 100 Hz. The test amplitude was set at 70 mV to make sure the precision of testing. The device was tested when the device turn-on, the measurement was done by three times, which are at voltage +3V, +4V, and +5V. The frequency sweep measurement result in a impedance (Z) cole-cole plot or usually called Nyquist plot. All of the measurements for the impedance spectroscopy were achieved in the room temperature ambient.

The purpose of the transient electroluminescence (TREL) measurement is to analyze the different responses when the device switches on and off. Some of the OLED devices, which have many traps or defects, can be resulting delays or spikes on the electroluminescence spectrum. This measurement is done by giving a pulse with a fixed voltage at +3 V, +4 V, +5 V, and +6 V. The pulse width is set at 100 μs, and the settling time is 10 μs. The TREL measurement is done at room temperature conditions. The data of this measurement is an electroluminescence spectrum, then needs to plot for the analyzing in the OriginPro software.

After all the device measurement is done, the data is collected and plotted to analyze the phenomenon inside each structure OLED. The result and discussion of this study will describe detail in Chapter 4.

Chapter 4 Result and Discussion

4.1 Optimization of Yellow Phosphorescent OLED

The optimization of yellow phosphorescent OLED (PhOLED) was done by choosing a donor-acceptor material for the exciplex system and fitting them with the new yellow emitter. The donor materials were BCzPh and TCTA, while the acceptor materials were CN-T2T and B3PYMPM. The exciplex system was mixed with the novel yellow phosphorescent dopant (Y1) with 4% and 8% dopant concentrations. This method is used to analyze the dopant concentration effect in OLED devices.

The OLED devices were fabricated as shown in Table 3.1 and Table 3.2. The optimization will be separated into two-phase; the application of BCzPh as donor material and the utilization of TCTA as donor material. All of the devices were measured by device performance measurement, photophysical performance, and electrical performance. The result and discussion of yellow PhOLED will be explained more in the next subchapter.

4.1.1 Device Performance Characterization

The first step of optimization of yellow PhOLED is using a BCzPh as donor materials. The BCzPh was mixed with two kinds of acceptor material which are CN-T2T and B3PYMPM. The exciplex was blended by Y1 dopant with 4% and 8% concentration. The device configuration of the BCzPh exciplex OLED is shown in Table 3.1. The EL device performance was plotted in the form of current density-voltage-luminance (JVL), current efficiency-power efficiency, external quantum efficiency, and EL spectrum, as depicted in Figure 4.1.

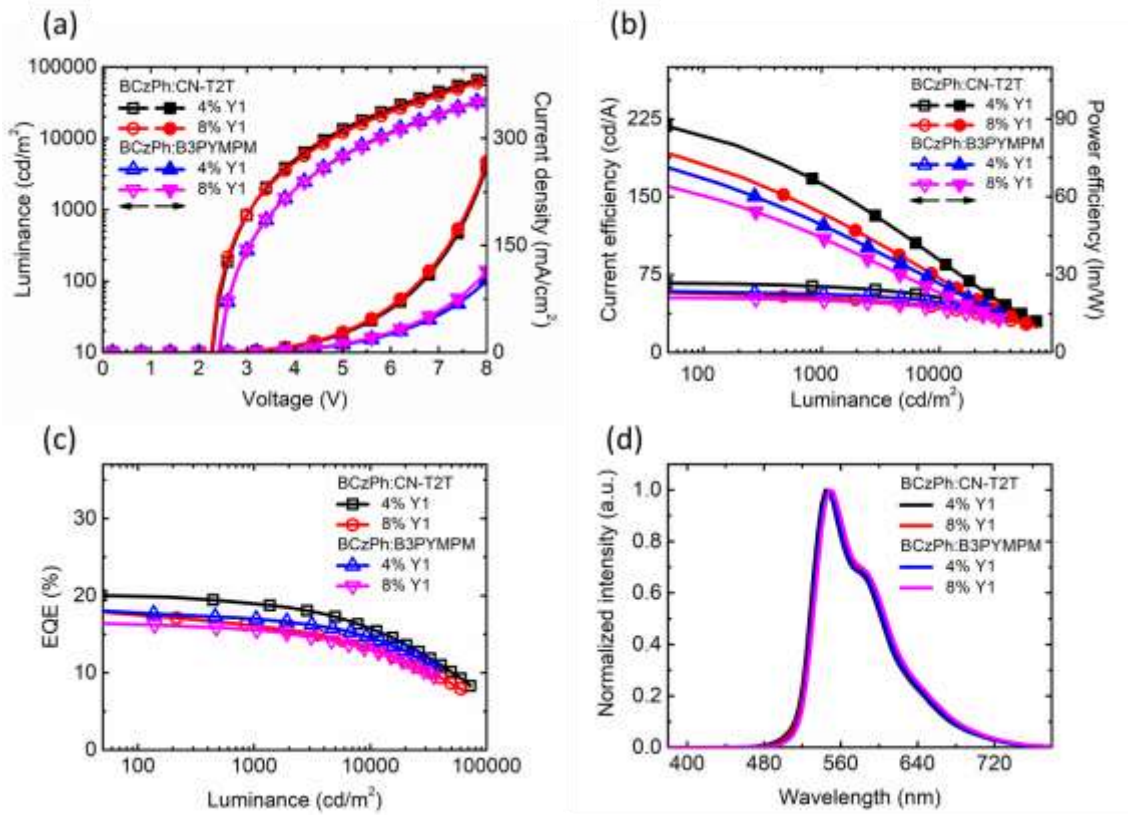

Figure 4.1 The BCzPh donor materials for Y1; (a) current density-voltage-luminance (JVL), (b) current efficiency-power efficiency, (c) EQE, (d) EL spectrum.

The EL characteristics data of BCzPh donor material for OLED devices was summarized in Table 4.1.

Table 4.1 The EL device performance of BCzPh donor material.

	V_{on}[a] [V]	L_{max} [cd m^{-2}]	η_c [cd A^{-1}]			η_p [lm W^{-1}]			η_{ext} [%]			$\eta_{roll\text{-}off}$[b,c] [%]	CIE @V_{max}
			max.	@1000 cd m^{-2}	@10000 cd m^{-2}	max.	@1000 cd m^{-2}	@10000 cd m^{-2}	max.	@1000 cd m^{-2}	@10000 cd m^{-2}		
BCzPh:CN-T2T: 4% Y1	2.4	72,640	66.69	62.81	51.69	87.30	61.66	33.83	20.02	18.74	15.41	6.39, 23.03	0.436, 0.552
BCzPh:CN-T2T: 8% Y1	2.4	66,520	57.66	51.89	43.35	75.48	50.95	28.37	17.75	15.86	13.19	10.65, 25.69	0.445, 0.546
BCzPh:B3PYMPM: 4% Y1	2.6	35,810	58.86	55.99	47.92	71.12	48.86	25.96	18.00	16.96	14.43	5.78, 19.83	0.455, 0.546
BCzPh:B3PYMPM: 8% Y1	2.6	35,390	52.80	50.18	42.07	63.80	43.79	22.79	16.39	15.54	12.93	5.19, 21.11	0.454, 0.538

[a] Defined at 100 cd m^{-2}.

[b] Compared the roll-off between the maximum and at 1000 cd m^{-2} of EQE.

[c] Compared the roll-off between the maximum and at 10000 cd m^{-2} of EQE.

Based on the result, the turn-on voltage of BCzPh mixed with CN-T2T acceptor material is lower than B3PYMPM materials. The BCzPh:CN-T2T mixed with 4% and 8% Y1 dopant has the same turn-on voltage of +2.4 V at 100 cd m^{-2}. Likewise, the BCzPh:B3PYMPM mixed with 4% and 8% Y1 has a turn-on voltage of +2.6 V at 100 cd m^{-2}. When we saw the HOMO-LUMO level of each acceptor material, there are almost don't have differences. According to Wang *et al.*, the HOMO level of CN-T2T is 2.7 eV, while the B3PYMPM is 2.8 eV. The LUMO level of CN-T2T is 6.7 eV, and B3PYMPM is 6.8 eV.[56] Therefore, the energy barrier difference between the device BCzPh with CN-T2T and the device BCzPh with B3PYMPM is not a reason for the differences in the turn-on voltage of the device.

One of the most reasons for the turn-on voltage differences is the mobility of the acceptor materials. Based on previous works in our lab, Lee *et al.* measured the electron mobility of B3PYMPM material of 6.49×10^{-7} cm^2 V^{-1} s^{-1} by SCLC measurement.[57] For the comparison, the electron mobility of CN-T2T is 9.4×10^{-5} cm^2 V^{-1} s^{-1} measured by *Hung et al.*[58] This result shows the device BCzPh mixed with CN-T2T has more charge balance than the device with B3PYMPM because of the higher electron mobility of the acceptor. The turn-on voltage was taken when the device was on at a luminance of 100 cd m^{-2}. So, the charge balance of the device can be considered as a reason. The device with higher mobility will have the lower turn-on voltage at 100 cd m^{-2}. If we compared with other works about a synthesized yellow phosphorescent dopant, the turn-on voltage of our work is the lowest one.[26,31] The lower turn-on voltage of this works is due to the utilization of the exciplex host system to improve the charge balance inside the EML layer. Besides that, the exciplex system also improves the turn-on voltage because exciplex is using an HTL and ETL

material as an emission layer, so there is no energy barrier between the transport and emission layer.

The maximum luminance (L_{max}) of BCzPh mixed with CN-T2T acceptor materials show superior results of 72,640 cd m^{-2} with a Commission Internationale de L'eclairage (CIE) coordinates of (0.436, 0.552) for 4% doping concentration, and 66,520 cd m^{-2} with CIE coordinates of (0.445, 0.546) for 8% Y1 dopant. However, the L_{max} of BCzPh mixed with B3PYMPM are 35,810 cd m^{-2} with the CIE of (0.455, 0.546) for 4% Y1 dopant, and 35,390 cd m^{-2} with the CIE of (0.454, 0.538) for 8% Y1 dopant. The higher luminance of BCzPh mixed with CN-T2T is caused by a higher current density than the B3PYMPM acceptor, as shown in Figure 4.1(a). The higher current density was resulting more charges will be injected into the emission layer which can be generating light. As explained before, the higher current density of BCzPh with CN-T2T devices is due to the higher mobility and charge balance.[57,58] The higher mobility will be causing the electrons and holes will be easier to flow inside of the materials.

As shown in Figure 4.1(b) and Figure 4.1(c), the maximum EQE (maximum CE, maximum PE) of BCzPh:CN-T2T:4% Y1, BCzPh:CN-T2T:8% Y1, BCzPh:B3PYMPM:4% Y1, and BCzPh:B3PYMPM:8% Y1 devices are 20.02% (66.69 cd A^{-1}, 87.30 lm W^{-1}), 17.75% (57.66 cd A^{-1}, 75.48 lm W^{-1}), 18.00% (58.86 cd A^{-1}, 71.12 lm W^{-1}), and 16.39% (52.80 cd A^{-1}, 63.80 lm W^{-1}). The best EQE was achieved by the BCzPh:CNT2T:4% Y1 devices. The impact of increasing dopant concentration was seen by slightly increasing the current density of the devices, as shown in Figure 4.1(a). The device with an 8% dopant concentration has a higher current density than the device with 4% dopant. The increment of dopant concentration in phosphorescent OLED can induce a carrier transport to outgrow, resulting in more Dexter electron energy transfer from host to

guest. In contrast, the EQE values of devices with 8% dopant concentration have lower performance than the 4% dopant, both for CN-T2T and B3PYMPM acceptor. The high doping concentration will make higher current density, which causing an imbalance charge inside EML, and resulting a lower EQE performance. Besides that, the high doping concentration would lead to a high chance of exciton decreased because of self-quenching by triplet-triplet annihilation (TTA).[59,60]

With the same doping concentration, the device BCzPh:CN-T2T:4% Y1 has a higher EQE value of 20.02% than the device BCzPh:B3PYMPM:4% Y1 of 18.00%. Better charge balance of the OLED devices will be affecting higher EQE value. The CN-T2T has higher electron mobility than B3PYMPM, so the device with CN-T2T has a better EQE value. The efficiency roll-off at 1,000 cd m^{-2} of BCzPh:CNT2T:4%Y1, BCzPh:CN-T2T:8%Y1, BCzPh:B3PYMPM:4% Y1, and BCzPh:B3PYMPM:8% Y1 are 6.39%, 10.65%, 5.78%, and 5.19%. Thus, the efficiency roll-off at 10,000 cd m^{-2} of BCzPh:CNT2T:4%Y1, BCzPh:CN-T2T:8%Y1, BCzPh:B3PYMPM:4% Y1, and BCzPh:B3PYMPM:8% Y1 are 23.03%, 25.69%, 19.83%, and 21.11%, as summarized in Table 4.1. The exciplex system helps OLED devices suppress an efficiency roll-off value due to better charge balance and high mobility. It is shown by low-efficiency roll-off at luminance 1,000 cd m^{-2} and 10,000 cd m^{-2} for all devices structure, is around 10% and 20%, respectively. Better charge balance with the utilization of high carrier mobility materials will decrease a carrier wasted for the formation of light.

The EL spectrum of each device is shown in Figure 4.1(d). It is shown the emission peak of all devices appears almost at the same wavelength peak around 545-550 nm. The result of the EL spectrum shows a similar trend for all device structures, which indicates all the energy was transferred to the phosphorescent dopant. The effect of increasing a dopant

concentration also impacts the red-shifted emission EL spectrum, as seen in Figure 4.1(d).

As the summary of the first optimization, the device BCzPh:CN-T2T:4% Y1 shows a superior result due to low turn-on voltage, high luminance, high EQE value, and low-efficiency roll-off. If we compared the result with other synthesized yellow phosphorescent dopant works, our works have a better device performance.[26–31] For the commercial yellow phosphorescent dopant, our OLED device performance showed a comparable result as another way to achieve the high EL performance of PhOLED.[23–25]

In Lee *et al.* works, they used a commercial yellow phosphorescent dopant (PO-01) mixed with one-off single host 3,3’’-di(9H-carbazol-9-yl)-[1,1’:2′,1’’-terphenyl]4′,5′-dicarbonitrile (IPNCz) and 3,3′-Di(9H-carbazol-9-yl)-1,1′-biphenyl (mCBP) host.[23] The EQE result is higher than our work, around 22-25% for them and 20% for us, but the maximum luminance of our work is better. The maximum luminance of our device is 72,640 cd m^{-2} at voltage +8 V, and the maximum luminance of them is 44,866 cd m^{-2} at voltage above +10 V. This result proved that the utilization of an exciplex system with a new synthesized phosphorescent dopant could be an alternative to achieve high EL device performance.

For next optimization of yellow PhOLED is using a TCTA as donor materials and mixed with one of CN-T2T and B3PYMPM. The exciplex was blended by Y1 dopant with 4% and 8% concentration. The device configuration of the TCTA exciplex OLED is shown in Table 3.2. The EL device performance was plotted in the form of current density-voltage-luminance (JVL), current efficiency-power efficiency, external quantum efficiency, and EL spectrum, as shown in Figure 4.2. The purpose of this part is to find another way for achieving a high EL performance using another hole transport material as a donor material in PhOLED devices.

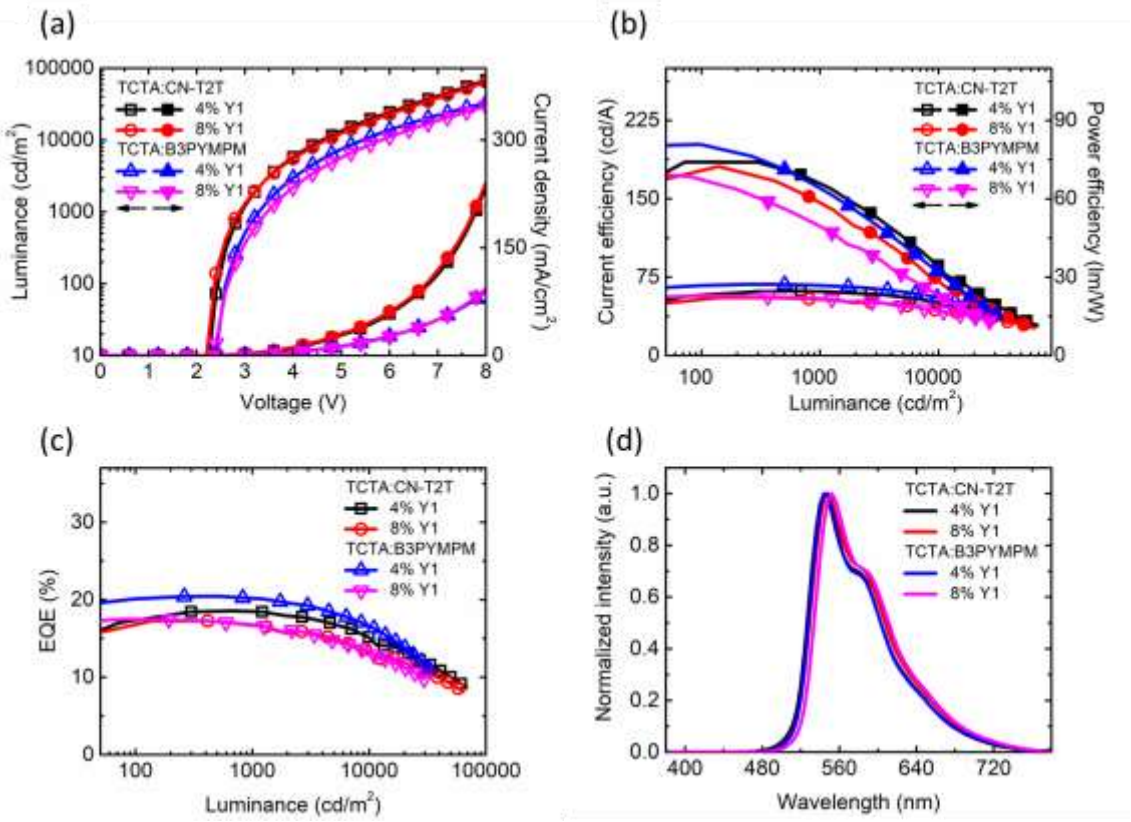

Figure 4.2 The TCTA donor materials for Y1; (a) current density-voltage-luminance (JVL), (b) current efficiency-power efficiency, (c) EQE, (d) EL spectrum.

The EL characteristics data of TCTA donor material for OLED devices was summarized in Table 4.2.

Table 4.2 The EL device performance of TCTA donor material.

	V_{on}[a] [V]	L_{max} [cd m^{-2}]	η_e [cd A^{-1}]			η_p [lm W^{-1}]			η_{ext} [%]			$\eta_{roll\text{-}off}$[b,c] [%]	CIE @V_{max}
			max.	@1000 cd m^{-2}	@10000 cd m^{-2}	max.	@1000 cd m^{-2}	@10000 cd m^{-2}	max.	@1000 cd m^{-2}	@10000 cd m^{-2}		
TCTA:CN-T2T: 4% Y1	2.4	68,260	61.69	61.34	50.33	69.21	66.13	34.31	18.57	18.48	15.11	0.48, 18.63	0.437, 0.551
TCTA:CN-T2T: 8% Y1	2.4	64,200	55.30	53.77	42.79	72.39	58.81	28.61	17.26	16.72	13.30	3.12, 22.94	0.449, 0.541
TCTA:B3PYMPM: 4% Y1	2.6	32,700	68.01	67.11	55.17	71.22	64.29	31.87	20.46	20.17	16.59	1.41, 18.91	0.440, 0.549
TCTA:B3PYMPM: 8% Y1	2.6	29,570	56.79	54.50	42.68	68.62	49.57	22.99	17.48	16.77	13.16	4.06, 24.71	0.450, 0.540

[a] Defined at 100 cd m^{-2}.

[b] Compared the roll-off between the maximum and at 1000 cd m^{-2} of EQE.

[c] Compared the roll-off between the maximum and at 10000 cd m^{-2} of EQE.

The turn-on voltage of TCTA:CN-T2T acceptor material is lower than TCTA:B3PYMPM. The TCTA:CN-T2T mixed with 4% and 8% Y1 dopant has the same turn-on voltage of +2.4 V at 100 cd m^{-2}. Likewise, the TCTA:B3PYMPM mixed with 4% and 8% Y1 has a turn-on voltage of +2.6 V at 100 cd m^{-2}. The explanation for this phenomenon is same with previous optimization, which CN-T2T has a higher electron mobility than the B3PYMPM materials.[57,58]

The maximum luminance (L_{max}) of TCTA:CN-T2T is 68,280 cd m^{-2} with CIE coordinates of (0.437, 0.551) for 4% Y1, and 64,200cd m^{-2} with CIE coordinates of (0.449, 0.541) for 8% Y1 dopant. Futhermore, the Lmax of TCTA:B3PYMPM are 32,700 cd m^{-2} with the CIE of (0.440, 0.549) for 4% Y1 dopant, and 29,570 cd m^{-2} with the CIE of (0.450, 0.540) for 8% Y1 dopant. The difference max luminance of CN-T2T and B3PYMPM devices was also from the higher current density of CN-T2T materials, as shown in Figure 4.2(a). But we need to highlight more about the maximum luminance from BCzPh device with TCTA devices. The BCzPh devices show a higher luminance than the TCTA devices. The best of BCzPh devices has a L_{max} of 72,640 cd m^{-2}, while the best of TCTA devices is 68,260 cd m^{-2}. According to this result, we find a reference that studies the hole mobility of each donor material. In our previous works, Lee *et al.* measured the hole mobility of BCzPh material of 1.09×10^{-5} cm^2 V^{-1} s^{-1} by SCLC measurement.[57] While Jiang *et al.* measured the hole mobility of TCTA material around 3.0×10^{-3} cm^2 V^{-1} s^{-1}.[61] The BCzPh hole mobility seen more balance if we compared with acceptor materials with the order of 10^{-5} than the TCTA in order of 10^{-3}. So, the maximum luminance of BCzPh devices looks higher than the TCTA because of the better hole and electron charge balance.

As shown in Figure 4.2(b) and Figure 4.2(c), the maximum EQE (maximum CE, maximum PE) of TCTA:CN-T2T:4% Y1, TCTA:CN-

T2T:8% Y1, TCTA:B3PYMPM:4% Y1, and TCTA:B3PYMPM:8% Y1 devices are 18.57% (61.69 cd A^{-1}, 69.21 lm W^{-1}), 17.26% (55.30 cd A^{-1}, 72.39 lm W^{-1}), 20.46% (68.01 cd A^{-1}, 71.22 lm W^{-1}), and 17.48% (56.79 cd A^{-1}, 68.62 lm W^{-1}). An effect of increasing the dopant concentration also can be seen in the improvement of the current density of the devices, as shown in Figure 4.2(a). Nevertheless, the increment of dopant concentration does not improve the EQE value due to the carrier imbalance with the increasing of current density of high doping concentration device. For the TCTA host system, the best EQE was shown by device TCTA:B3PYMPM:4% Y1 with 20.46%. The performance of this device has a great EQE value, but from a luminance point of view, the device TCTA:CN-T2T:4% Y1 has the best one with 68,260 cd m^{-2} and EQE of 18.57%. Therefore, there are two kinds of structures, each having its advantages depending on its applications. TCTA:CN-T2T:4% Y1 has high maximum luminance, but the EQE value is not high enough, while TCTA:B3PYMPM:4% Y1 has a high EQE value, but the L_{max} is not so high.

The EL emission peak of all devices appears almost at the same wavelength peak around 545-550 nm, as shown in Figure 4.2(d). The result of the EL spectrum shows a similar trend with a single peak emission, which indicates all the energy was transferred to the phosphorescent dopant. The red-shifted EL spectrum is due to increasing the dopant concentration in the devices.

As summarized in Table 4.2, all devices have low-efficiency roll-off at luminance 1,000 cd m^{-2} and 10,000 cd m^{-2} for all devices structure, is around 10% and 20%, respectively. In a high current density situation, having a better charge balance helps OLED devices suppress an efficiency roll-off value to decrease wasted electron and hole pairs from generating light.

4.1.2 Photophysical Characterization

The photophysical measurement is used to analyze the exciplex formation characteristics. The photophysical characterization of BCzPh as donor materials are depicted in Figure 4.3. The emission spectrum of a single donor and acceptor molecules shows a peak centered at 415 nm (BCzPh), 403 nm (CN-T2T), 397 nm (B3PYMPM). Whereas, the PL spectra of the exciplex host exhibit a distinct emission peak at 523 nm (BCzPh:CN-T2T) and 485 nm (BCzPh:B3PYMPM) without any peaks correlated with the component materials. This result explicitly indicates the exciplex was formed in the devices.[16,41] The PL spectra for exciplex host mixed Y1 dopant with various doping concentrations also was observed, as shown in Figure 4.3(a). The results show all PL spectra have a single peak around 445-450 nm, which is very different from the exciplex host peaks, explaining that all energy was transferred and the PL emission is only from the dopant.[16] The higher doping concentration effects were also seen in PL spectra emission. The exciplex with 8% doping concentration has a red-shifted emission spectrum than the 4% dopant.

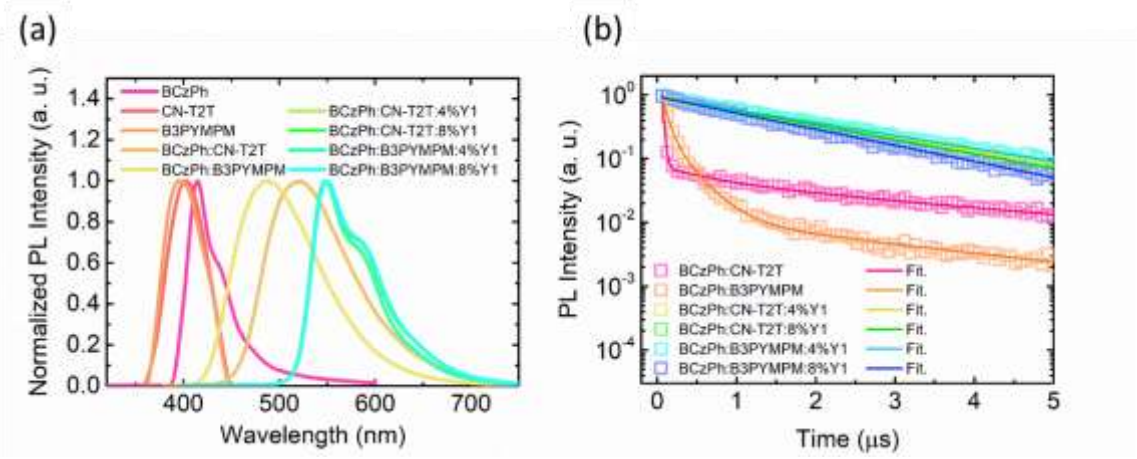

Figure 4.3 The photophysical characterization of BCzPh as donor; (a) PL spectra and (b) TRPL

The time-resolved photoluminescence (TRPL) measurement of BCzPh as a donor material also could be seen in Figure 4.3(b). The parameter of each TRPL measurement was summarized in Table 4.3 and Table 4.4. The PL decay profile of BCzPh:CN-T2T exciplex could be fitted with two parameters, which are prompt (T_1) of 22.59 ns and delayed fluorescence (T_2) of 3.6 μs. Moreover, the decay profile of BCzPh:B3PYMPM has a prompt of 72.07 ns and delayed fluorescence of 2.8 μs. Both of the exciplex hosts have a delayed fluorescence profile, which indicates the TADF works in this system. The delayed fluorescence profile of BCzPh:B3PYMPM is lower than the BCzPh:CN-T2T profile due to insufficient exciplex formation within the device.[41]

When the Y1 dopant was blended with the exciplex systems, the prompt profile does not appear in the TRPL result, which exhibits the energy transfer was fully transferred to the phosphorescence dopant.[16] The delayed fluorescence profile of exciplex host mixed with Y1 dopant is recapped in Table 4.3. The higher doping concentration will cause a lower delayed fluorescence profile in the TRPL result.

Table 4.3 The PLQY and TRPL lifetime of exciplex host with Y1 dopant.

Exciplex	Y1 Doping Ratio [wt.%]	PLQY @320 nm [%]	TRPL Lifetime [ns]
BCzPh:CN-T2T	4	74	2133.32
BCzPh:CN-T2T	8	67	1915.10
BCzPh:B3PYMPM	4	70	2140.10
BCzPh:B3PYMPM	8	62	1712.60
TCTA:CN-T2T	4	73	2288.13
TCTA:CN-T2T	8	63	1956.94
TCTA:B3PYMPM	4	68	2107.06
TCTA:B3PYMPM	8	67	1725.32

Table 4.4 The summary of TRPL decay parameter of exciplex host.

Exciplex	T_1 [ns]	T_2 [ns]
BCzPh:CN-T2T	22.59	3640.42
BCzPh:B3PYMPM	72.07	2774.90
TCTA:CN-T2T	40.00	4256.90
TCTA:B3PYMPM	102.78	2211.65

In the TCTA host system, the PL spectra and TRPL result is shown in Figure 4.4. The exciplex system TCTA:CN-T2T has a single peak at 539 nm, while TCTA:B3PYMPM system has a peak at 503 nm, which is dissimilar with the component materials TCTA (centered at 385 nm), CN-T2T(centered at 403 nm), and B3PYMPM (centered at 397 nm). The new PL emission with the absence of a single component emission is a good indication of exciplex formation under photoexcitation.[16] The PL spectra for exciplex host mixed Y1 dopant is shown in Figure 4.4(b). All of the PL spectra of exciplex mixed with Y1 dopant show an emission peak around 545-550 nm, which indicates the energy was transferred to the phosphorescent dopant. The effect of higher doping concentration also can be seen in the TCTA systems. The red-shifted emission was shown both in PL spectra and EL spectrum which proves the phenomenon.

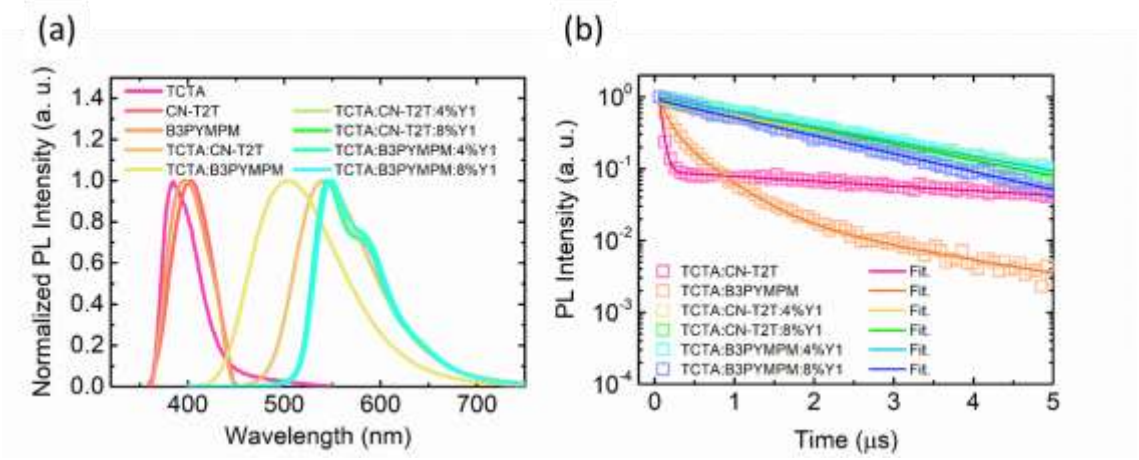

Figure 4.4 The photophysical characterization of TCTA as donor; (a) PL spectra and (b) TRPL

The TRPL measurement of TCTA systems are depicted in Figure 4.4(b). The parameter of TRPL measurement was shown in Table 4.3 and Table 4.4. The decay profile of TCTA:CN-T2T exciplex was fitted by two parameters, which are prompt (T_1) of 40.00 ns and delayed fluorescence (T_2) of 4.3 µs. While the decay profile of TCTA:B3PYMPM has a prompt of 102.78 ns and a delayed fluorescence of 2.2 µs. The delayed fluorescence profile of TCTA:B3PYMPM is lower than the TCTA:CN-T2T profile due to insufficient exciplex formation within the device.[41] The delayed fluorescence profiles of the exciplex system are a good reason for exciplex formation in the devices.

The TRPL results of TCTA exciplex systems were mixed with 4% and 8% Y1 dopant are shown in Figure 4.4(b). The prompt profile of the TCTA exciplex host mixed with Y1 dopant does not appear in the TRPL response. This result shows the energy was fully transferred to the phosphorescent dopant.[16] The TRPL lifetime of the TCTA exciplex system mixed with 4% and 8% Y1 dopant is recapped in Table 4.3. The effect of higher doping concentration will be affected a lower delayed fluorescence profile in the TRPL result.

The photoluminescence quantum yield (PLQY) measurements results of the BCzPh and TCTA exciplex hosts blended with Y1 dopant were summarized in Table 4.3. The highest PLQY value is shown by BCzPh:CN-T2T:4% Y1 with 74%. As shown in Table 4.3, the CN-T2T materials as an acceptor in the exciplex system have a higher PLQY value than the B3PYMPM materials. This is one of the explanations why the exciplex system with CN-T2T has a higher EL performance than B3PYMPM. Besides that, the higher dopant concentration will be affecting a lowering the PLQY value of all exciplex systems. This phenomenon will cause the EQE of high doping concentration devices to be lower than the low doping concentration devices.

4.1.3 Electrical Characterization

The electrical characterization was displayed by capacitance-voltage (CV) plots and impedance cole-cole plots. The CV plots were used to examine the charge dynamic inside the devices. While the impedance cole-cole was used to analyze the accumulation charge inside the device under different applied biases. The result and discussion of electrical characterization will be explained below.

A. Capacitance-voltage (CV) plots

The capacitance-voltage (CV) plots are divided into four areas under applied bias. All of the devices (BCzPh and TCTA as donor material, CN-T2T and B3PYMPM as acceptor material) were measured by sweeping the applied bias from +0 - +6V with a fixed frequency. The CV plot result is shown in Figure 4.5(a) for BCzPh, and Figure 4.5(b) for TCTA.

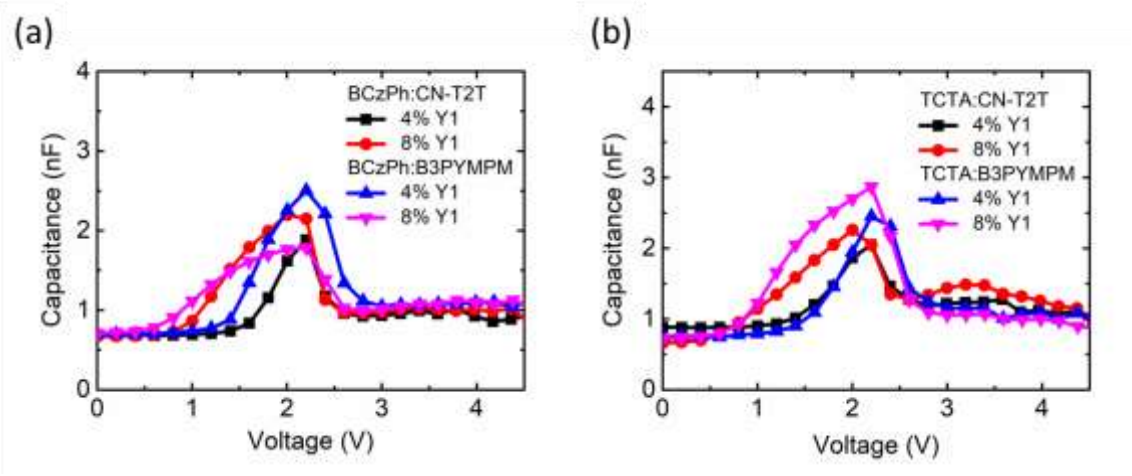

Figure 4.5 The capacitance-voltage (CV) plot of; (a) BCzPh, (b) TCTA.

The first part is $V_0 < V_t$, which means the carrier is not injected into the devices, in other words, the devices behave like an insulating dielectric between two electrodes.[41] The threshold voltage (V_t) for BCzPh:CN-T2T:4%Y1, BCzPh:CN-T2T:8%Y1, BCzPH:B3PYMPM:4%Y1, and BCzPh:B3PYMPM:8% Y1 are 1.2 V, 0.6 V, 1.2V, and 0.6V. In addition, the threshold voltage for TCTA:CN-T2T:4% Y1, TCTA:CN-T2T:8% Y1,

TCTA:B3PYMPM:4% Y1, and TCTA:B3PYMPM:8% Y1 are 1.2 V, 0.6 V, 1.2 V, 0.6 V.

The next part is when $V_0 = V_t$, which means the applied bias (V_0) was achieved the threshold voltage, so the charge wants start to inject into the devices. From this V_t value, we can assume that there are no differences in the energy barrier which causes dissimilarity of the threshold voltage of the devices. By increasing the doping concentration from 4% to 8% can help for decreasing the threshold voltage. After that, the value of V_0 will be higher than V_t ($V_t < V_0 < V_{bi}$). The carrier will be injected more and marked by the capacitance value increase. The charge injection will be done until the applied voltage (V_0) reach the built-in voltage (V_{bi}).

The built-in voltage (V_{bi}) of BCzPh:CN-T2T:4%Y1, BCzPh:CN-T2T:8%Y1, BCzPH:B3PYMPM:4%Y1, and BCzPh:B3PYMPM:8% Y1 are 2.2 V, 2.0 V, 2.2 V, 2.2 V. The built-in voltage (V_{bi}) of TCTA:CN-T2T:4%Y1, TCTA:CN-T2T:8%Y1, TCTA:B3PYMPM:4%Y1, and TCTA:B3PYMPM:8% Y1 are 2.2 V, 2.0 V, 2.2 V, 2.2 V. After reaching a built-in voltage ($V_0 > V_{bi}$), the capacitance response will decrease faster, indicating the charge in the device was recombined and generated light.

B. Impedance cole-cole (Z) plots

The impedance cole-cole plots were used to analyze the accumulation charge inside the OLED under applied voltages. The impedance cole-cole for BCzPh devices were shown in Figure 4.6, and for TCTA devices were shown in Figure 4.7. All of the devices were fitted with an equivalent RC circuit as shown in Figure 2.15. The resistor and capacitor value of the equivalent circuit was summarized in Table 4.5 for BCzPh devices, and Table 4.6 for TCTA devices. The impedance plot was measured at turn-on light conditions or at an applied voltage of +3 V, +4 V, and +5 V.

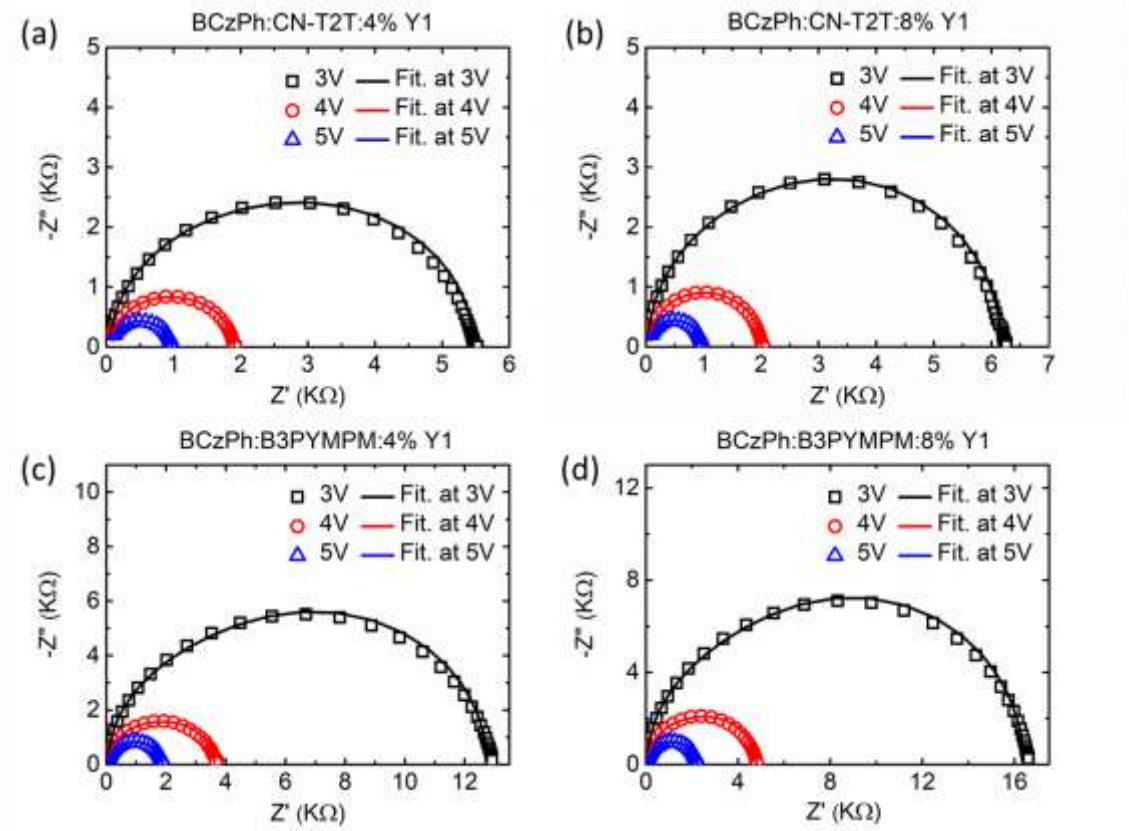

Figure 4.6 The impedance cole-cole plot of; (a) BCzPh:CN-T2T:4% Y1, (b) BCzPh:CN-T2T:8% Y1, (c) BCzPh:B3PYMPM:4% Y1, (d) BCzPh:B3PYMPM:8% Y1.

Table 4.5 The parameter of equivalent circuit BCzPh donor material.

	Voltage [V]	R_S [Ω]	R_1 [Ω]	C_1 [nF]	R_2 [Ω]	C_2 [nF]
BCzPh:CN-T2T :4% Y1	3	61.2	1931 ± 139	1.18 ± 0.04	3471 ± 138	1.84 ± 0.12
	4	61.2	1140 ± 49	0.89 ± 0.02	704 ± 49	3.69 ± 0.04
	5	61.2	679 ± 27	0.82 ± 0.02	235 ± 27	5.66 ± 0.98
BCzPh:CN-T2T :8% Y1	3	36.6	1643 ± 167	1.44 ± 0.08	4493 ± 165	1.45 ± 0.09
	4	36.6	1257 ± 69	0.89 ± 0.03	729 ± 68	3.85 ± 0.56
	5	36.6	656 ± 42	0.86 ± 0.04	283 ± 42	4.29 ± 0.90
BCzPh:B3PYMPM :4% Y1	3	51.4	3126 ± 184	1.66 ± 0.06	9573 ± 180	1.36 ± 0.04
	4	51.4	1649 ± 117	1.04 ± 0.04	1931 ± 114	2.53 ± 0.25
	5	51.4	638 ± 46	0.88 ± 0.02	1200 ± 46	4.50 ± 0.52
BCzPh:B3PYMPM :8% Y1	3	49.6	3638 ± 185	1.38 ± 0.03	12704 ± 180	1.60 ± 0.05
	4	49.6	2007 ± 111	1.07 ± 0.03	2748 ± 110	2.34 ± 0.16
	5	49.6	1440 ± 46	0.90 ± 0.02	761 ± 45	4.92 ± 0.50

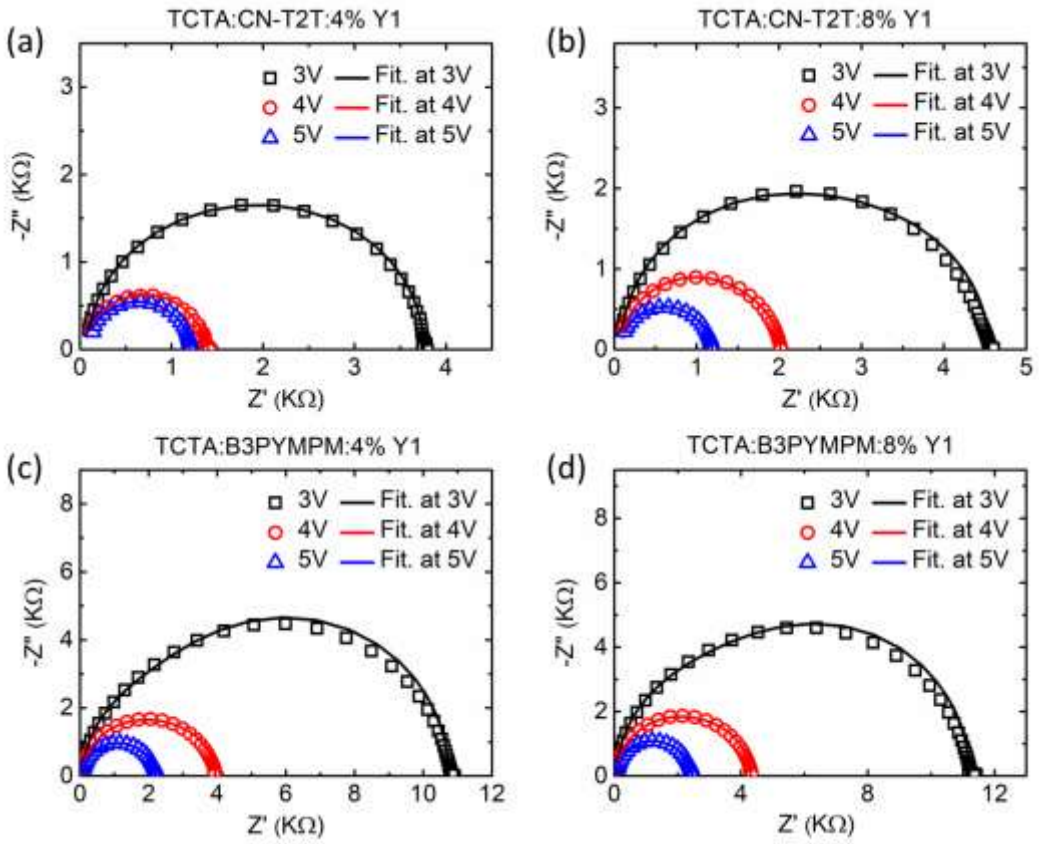

Figure 4.7 The impedance cole-cole plot of; (a) TCTA:CN-T2T:4% Y1, (b) TCTA:CN-T2T:8% Y1, (c) TCTA:B3PYMPM:4% Y1, (d) TCTA:B3PYMPM:8% Y1.

Table 4.6 The parameter of equivalent circuit TCTA donor material.

	Voltage [V]	R_S [Ω]	R_1 [Ω]	C_1 [nF]	R_2 [Ω]	C_2 [nF]
TCTA:CN-T2T :4% Y1	3	81.9	1657 ± 78	1.01 ± 0.03	2019 ± 77	2.12 ± 0.13
	4	81.9	1238 ± 10	0.73 ± 0.01	177 ± 10	8.16 ± 0.25
	5	81.9	962 ± 140	0.69 ± 0.07	162 ± 13	9.18 ± 0.14
TCTA:CN-T2T :8% Y1	3	78.9	2622 ± 102	0.83 ± 0.08	1844 ± 101	1.40 ± 0.15
	4	78.9	1635 ± 17	0.71 ± 0.01	304 ± 17	2.52 ± 0.04
	5	78.9	101 ± 7	0.69 ± 0.01	107 ± 8	3.60 ± 0.34
TCTA:B3PYMPM :4% Y1	3	86.5	2155 ± 75	1.25 ± 0.02	8502 ± 75	1.67 ± 0.03
	4	86.5	1624 ± 67	0.87 ± 0.01	2232 ± 68	3.84 ± 0.28
	5	86.5	434 ± 32	0.76 ± 0.01	1692 ± 32	9.80 ± 1.28
TCTA:B3PYMPM :8% Y1	3	81.1	3130 ± 111	1.11 ± 0.02	7999 ± 110	1.90 ± 0.06
	4	81.1	2597 ± 81	0.83 ± 0.01	1630 ± 81	4.08 ± 0.35
	5	81.1	1953 ± 26	0.73 ± 0.01	430 ± 26	11.9 ± 1.33

The impedance cole-cole plots were depicted as a semicircle diameter of impedance. Decreasing the semicircle diameter of impedance can indicate more light was generated. All of the figure plots show the same trend where the semicircle diameter decrease as the applied voltage increased, explicitly indicating more light generated from the device.

The equivalent circuit of the OLED devices can be represented as a series connection of a single resistor and two parallel RC circuits, as shown in Figure 2.15. The two parallel RC circuits are constructed due to the device containing two regions with differential electrical behavior.[50-51] First RC (R_1, C_1) parallel in the equivalent circuits is representative of one electrical behavior, which is hole conduction behavior (p-type materials). Then, the next RC (R_2, C_2) parallel is considered as an electron conduction behavior (n-type materials). Whereas the series resistance (R_s) is considered the contact resistance between the organic materials and the metal.

Then, The impedance cole-cole plots were fitted with the chosen equivalent circuits, and the fitted result is shown in Figure 4.6 and Figure 4.7. The equivalent circuit component was summarized in Table 4.5 and Table 4.6. The high doping concentration effect in OLED devices can be lowering the sheet resistance of equivalent circuits. The series resistance (R_s) as a voltage increase of each device was fixed in the fitting system, it is due to the assumption of the same value of internal resistance of organic materials between two electrodes. All of the R_1, C_1, and R_2 values is decrease with the increase in the applied bias for BCzPh and TCTA devices. However, the C_2 values increase along with increasing the voltage.

To see the impact of each structure for impedance value, we plotted impedance for all devices in one figure at +4 V applied bias. The impedance plot at +4 V is depicted in Figure 4.8(a) for BCzPh devices, and Figure 4.8(b) for TCTA devices. The differences of each device can be seen with the semicircle size of impedance value. The smaller size will be

better for the device, which means more light is generated. From the result, both the BCzPh and TCTA device with CN-T2T has a lower semicircle size than the device with B3PYMPM. That means more light is generated from devices with CN-T2T as acceptor materials, it proved by higher maximum luminance of CN-T2T devices as acceptor material. Moreover, the doping concentration effect also correlated with the impedance result. The high doping concentration of each device will make the bigger semicircle size of impedance values, which affects a lower luminance.

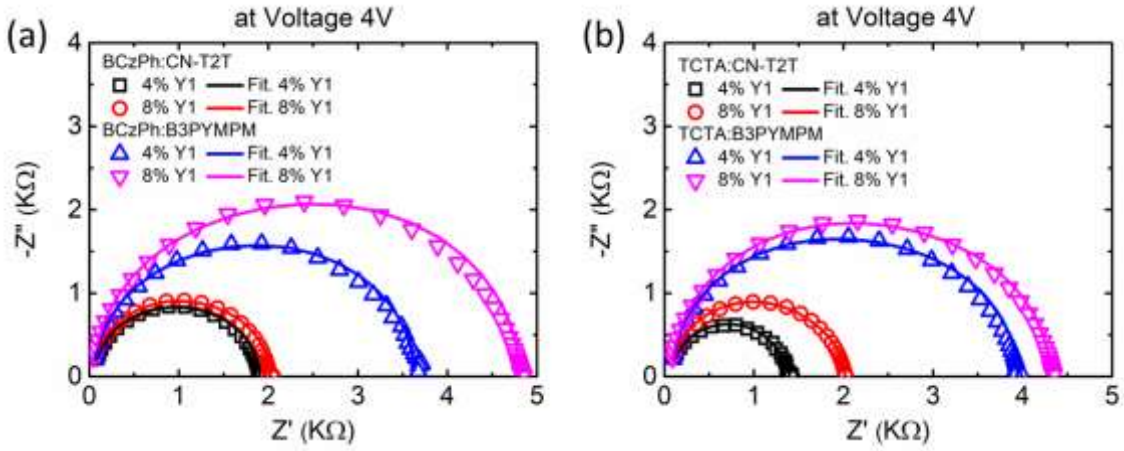

Figure 4.8 The impedance cole-cole plot at voltage +4 V of; (a) BCzPh (b) TCTA.

4.1.4 Transient Electroluminescence Characterization

The transient electroluminescence (TREL) plot has two main parts that need to be observed, which are the rising part and the decayed part. This measurement was a reliable tool to study the charge injection, recombination, and trapped charge inside the device. The TREL result for BCzPh devices was shown in Figure 4.9(a) and Figure 4.9(b) for the decay part. The TREL response was taken at +6 V bias when the turn-on condition.

For BCzPh devices, the rising time of device BCzPh:CN-T2T shows a shorter time than BCzPh:B3PYMPM devices, which means the devices with CN-T2T as an acceptor material has a better charge injection and transportation into EML layer for generating light. The rising EL profile exhibit a slight overshoot peak verifying strong injection at the turn-on condition. The doping concentration effect also can be seen here, the device with a high doping concentration will take a longer time to generate light. It is because the charge is injected into high doping concentration devices that could be degenerated by the self-quenching process so will delay generating light.[59,60] The slight overshoot peak was also seen a few microseconds after turn-off the bias voltage. It could be due to the trapped charge inside the emitting layer, which accumulated during the turn-on condition. As shown in Figure 4.9(b), the short decay time value was seen around 6-7 μs for all devices, indicating the low trap density in the devices.

The TREL result for TCTA devices was shown in Figure 4.9(c) and Figure 4.9(d). As the result, the device with CN-T2T as acceptor material has a better charge injection and transportation to the EML layer than the B3PYMPM materials. The doping concentration-effect also can be seen in this system, which causes a longer rising time. The rising EL profile exhibit a slight overshoot peak which indicates a good injection at the turn-on condition. But, the device TCTA:CN-T2T:8% Y1 look has a higher overshoot peak, which could be due to the initial charge inside the devices and affected higher peak in emission a light. The decay time which is shown in Figure 4.9(d) has a value of around 6-7 μs for all devices showing de-trapped charge carriers' release.

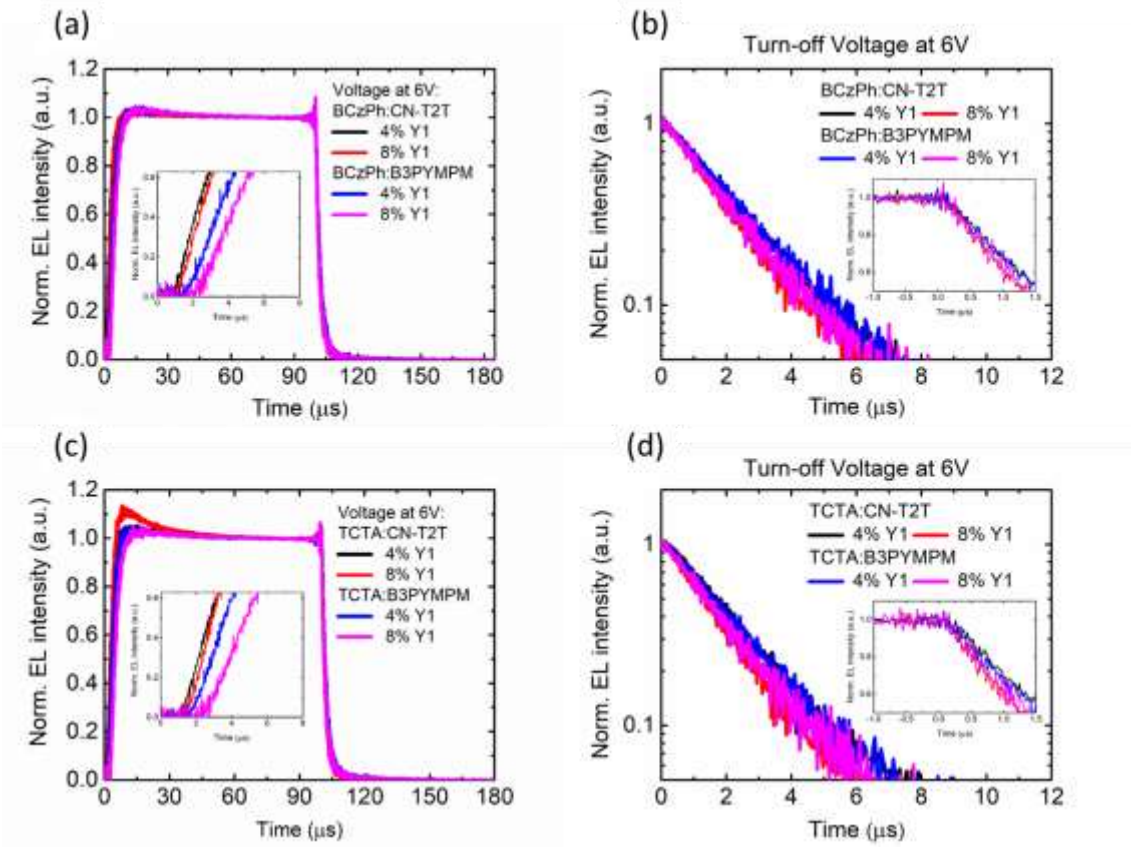

Figure 4.9 The transient electroluminescence response of; (a) BCzPh, (b) EL decay part of BCzPh, (c) TCTA, (d) EL decay part of TCTA.

4.2 Optimization of Red Phosphorescent OLED

For the red phosphorescent OLED, the basic structure was the same using BCzPh or TCTA as donor materials and CN-T2T and B3PYMPM as acceptor materials. The differences are only the dopant, we are using R1 and R2 dopant to see the OLED device performance as a solution in red PhOLED applications. The exciplex system was mixed with 4% and 8% dopant concentrations.

4.2.1 Device Performance Characterization

The first red phosphorescent dopant (R1) was tested by BCzPh basic structure, as shown in Table 3.1. Additionally, the red dopant (R2) was fabricated by TCTA basic structure, as shown in Table 3.2.

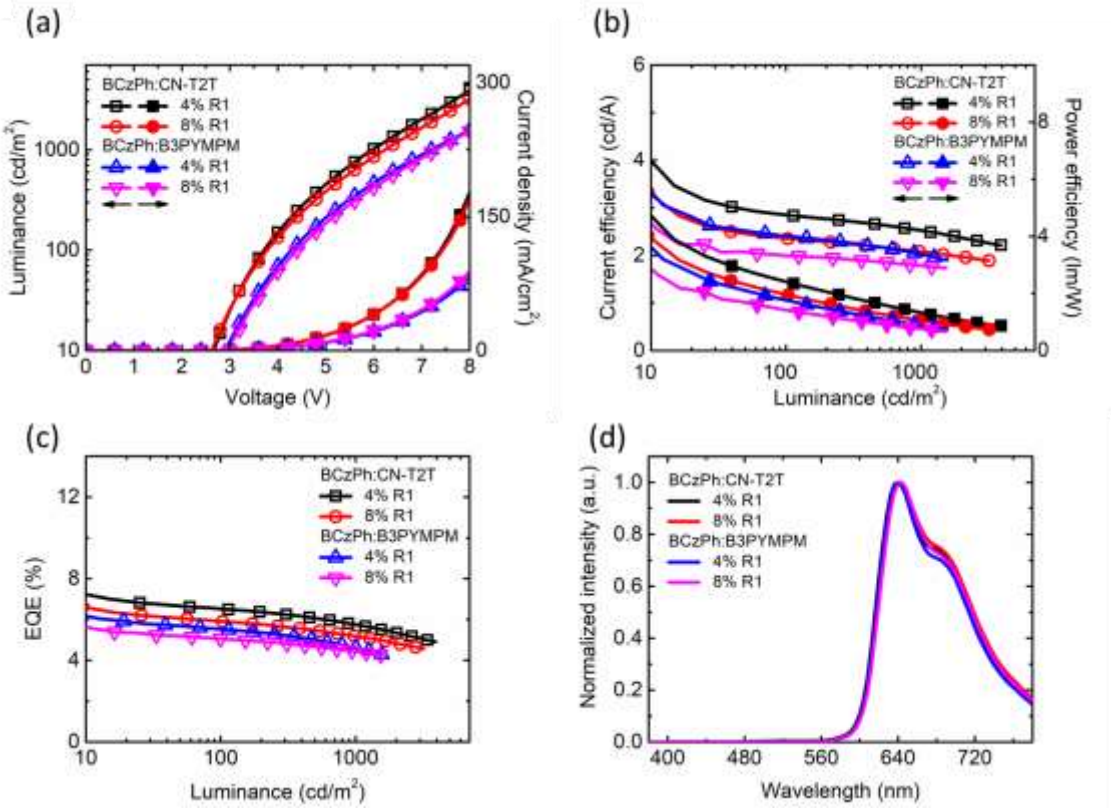

Figure 4.10 The BCzPh as donor materias for R1; (a) current density-voltage-luminance (JVL), (b) current efficiency-power efficiency, (c) EQE, (d) EL spectrum.

The EL characteristics data of BCzPh as donor material for red phosphorescent (R1) OLED devices was summarized in Table 4.7.

Table 4.7 The EL device performance of TCTA donor material.

	V_{on}[a] [V]	L_{max} [cd m^{-2}]	η_c [cd A^{-1}]			η_p [lm W^{-1}]			η_{ext} [%]			$\eta_{roll\text{-}off}$[b] [%]	CIE @V_{max}
			max.	@1000 cd m^{-2}	@10000 cd m^{-2}	max.	@1000 cd m^{-2}	@10000 cd m^{-2}	max.	@1000 cd m^{-2}	@10000 cd m^{-2}		
BCzPh:CN-T2T: 4% R1	3.7	3,925	4.23	2.52	n/a	5.11	1.32	n/a	7.01	5.74	n/a	18.11	0.691, 0.307
BCzPh:CN-T2T: 8% R1	3.7	2,793	3.33	2.08	n/a	4.02	1.05	n/a	6.35	5.19	n/a	18.27	0.697, 0.303
BCzPh:B3PYMPM: 4% R1	4.3	1,564	3.64	2.02	n/a	4.08	0.88	n/a	6.05	4.63	n/a	23.47	0.696, 0.303
BCzPh:B3PYMPM: 8% R1	4.3	1,537	2.99	1.78	n/a	3.35	0.76	n/a	5.56	4.42	n/a	20.50	0.699, 0.301

[a] Defined at 100 cd m^{-2}.

[b] Compared the roll-off between the maximum and at 1000 cd m^{-2} of EQE.

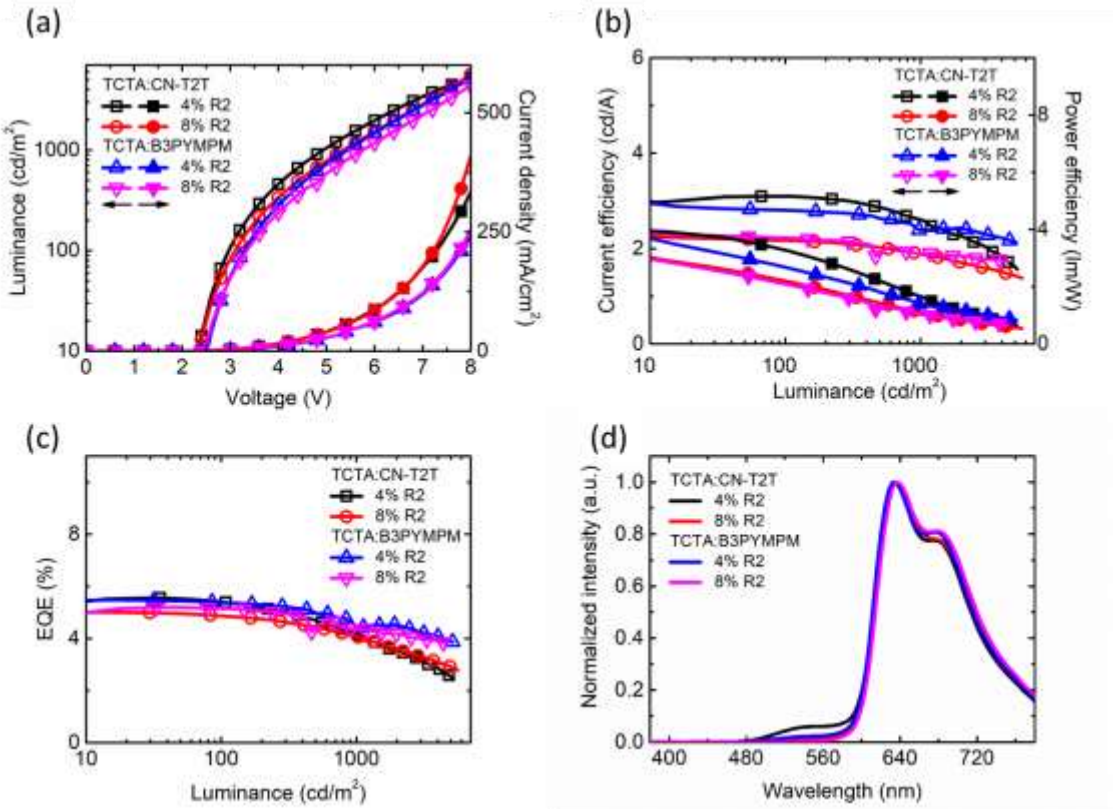

Figure 4.11 The TCTA as donor materias for R2; (a) current density-voltage-luminance (JVL), (b) current efficiency-power efficiency, (c) EQE, (d) EL spectrum.

The EL characteristics data of TCTA as donor material for red phosphorescent (R2) OLED devices was summarized in Table 4.8.

Table 4.8 The EL device performance of TCTA donor material.

	V_{on}[a] [V]	L_{max} [cd m^{-2}]	η_c [cd A^{-1}]			η_p [lm W^{-1}]			η_{ext} [%]			$\eta_{roll\text{-}off}$[b] [%]	CIE @V_{max}
			max.	@1000 cd m^{-2}	@10000 cd m^{-2}	max.	@1000 cd m^{-2}	@10000 cd m^{-2}	max.	@1000 cd m^{-2}	@10000 cd m^{-2}		
TCTA:CN-T2T: 4% R2	3.0	5,200	3.08	2.60	n/a	3.72	1.66	n/a	5.56	4.17	n/a	25.00	0.644, 0.349
TCTA:CN-T2T: 8% R2	3.0	5,643	2.21	1.89	n/a	2.67	1.11	n/a	4.99	4.07	n/a	18.44	0.681, 0.316
TCTA:B3PYMPM: 4% R2	3.3	5,142	2.88	2.38	n/a	3.48	1.38	n/a	5.48	4.48	n/a	17.92	0.671, 0.325
TCTA:B3PYMPM: 8% R2	3.3	4,397	2.25	1.89	n/a	2.35	1.03	n/a	5.20	4.34	n/a	16.54	0.692, 0.307

[a] Defined at 100 cd m^{-2}.

[b] Compared the roll-off between the maximum and at 1000 cd m^{-2} of EQE.

The device performance characterization is shown in Figure 4.10 for R1 dopant and Figure 4.11 for R2 dopant. All of the parameters was recapitulated in Table 4.7 for R1 dopant and Table 4.8 for R2 dopant. For the first phosphorescent dopant (R1), the turn-on voltage of BCzPh:CN-T2T:4%R1 and BCzPh:CN-T2T:8%R1 are 3.7 V, while the turn-on voltage BCzPh:B3PYMPM:4%R1 and BCzPh:B3PYMPM:8%R1 are 4.3 V. Moreover, the turn-on voltage of TCTA:CN-T2T:4%R2 and TCTA:CN-T2T:8%R2 are 3.0 V, while the turn-on voltage TCTA:B3PYMPM:4%R2 and TCTA:B3PYMPM:8%R2 are 3.3 V. All of the turn-on voltages was taken at luminance of 100 cd m^{-2}.

The maximum EQE (maximum CE, maximum PE) of BCzPh:CN-T2T:4% R1, BCzPh:CN-T2T:8% R1, BCzPh:B3PYMPM:4% R1, and BCzPh:B3PYMPM:8% R1 devices are 7.01% (4.23 cd A^{-1}, 5.11 lm W^{-1}), 6.35% (3.33 cd A^{-1}, 4.02 lm W^{-1}), 6.05% (3.64 cd A^{-1}, 4.08 lm W^{-1}), and 5.56% (2.99 cd A^{-1}, 3.35 lm W^{-1}). Whereas, for the TCTA:CN-T2T:4% R2, TCTA:CN-T2T:8% R2, TCTA:B3PYMPM:4% R2, and TCTA: B3PYMPM:8% R2 devices are 5.56% (3.08 cd A^{-1}, 3.72 lm W^{-1}), 4.99% (2.21 cd A^{-1}, 2.67 lm W^{-1}), 5.48% (2.88 cd A^{-1}, 3.48 lm W^{-1}), and 5.20% (2.25 cd A^{-1}, 2.35 lm W^{-1}). All devices with red dopant R1 and R2 show a very low luminance below 10,000 cd m^{-2} at +8 V. The best luminance only from device TCTA:CN-T2T:8% R2 with 5,643 cd m^{-2}. The efficiency roll-off for all devices is also high enough with around 20% at a luminance of 1,000 cd m^{-2}. In summary of red PhOLED, the performance of all devices with a novel red phosphorescent dopant R1 and R2 generate unsatisfactory performance. We think the problem is from the red dopant, which was synthesized. Because the basic structure of the exciplex system as a co-host works very well in yellow dopant with superior EL performance. Thus, the red synthesized phosphorescent dopant needs to study more to improve the EL performance in the future.

Chapter 5 Conclusions

5. Conclusions

In summary, we study the optimization of phosphorescent OLED using various bulk exciplex systems with a new synthesized yellow and red dopant. Each structure of OLED devices was examined by device characterization, photophysical characterization, and electrical characterization.

- In the exciplex system, the charge balance of electrons and holes inside the device can influence the EL performance of OLED. This statement was supported by the devices with CN-T2T as acceptor materials in exciplex show better performance (low turn-on voltage, high EQE, high luminance, low efficency roll-off) than the B3PYMPM materials due to better charge balance in the EML layer.
- In yellow phosphorescent dopant, the effect of high doping concentration can induce a carrier transport to outgrow, seen in higher current density. However, the device with 8% dopant has a lower EL performance than devices with 4%, it's because the high dopant makes a high chance the exciton can be disappeared by self-quenching mechanism. In addition, the high doping will make the red-shifted emission spectrum of OLED, which showed in the EL and PL spectra results.
- For the photophysical characterization, all of the exciplex systems show a new PL emission spectrum, which is different from the single component composer. This result proves that exciplex has formed inside the devices. The exciplex systems also have two decay profiles in the TRPL result, which indicates the exciplex behavior. The energy transfer between the exciplex and dopant is shown in the

new single peak PL emission and one decay profile of the TRPL result.

- For the electrical characterization, the CV plots show all devices have a four-part parameter under a bias. The Vt and Vbi was the main parameter for analyzing the CV plots data. The impedance cole-cole plot of devices at +3 V bias holds more capacitance. As voltage increases, the semicircle diameter of impedance will decrease and indicating more light was generated. The better charge balance inside devices will make the semicircle diameter smaller, as shown in devices with CN-T2T as an acceptor material.
- For the red phosphorescent OLED, the devices blended with the R1 and R2 dopants exhibit weak EL performances. Nevertheless, the exciplex system works very well in yellow phosphorescent OLED. Thus, the red phosphorescent dopants (R1 and R2) need more in-depth study for the OLED applications.

References

[1] C.W. Tang, S.A. Vanslyke, Organic electroluminescent diodes, Appl. Phys. Lett. 51 (1987) 913–915. https://doi.org/10.1063/1.98799.

[2] Y. Jeon, H.R. Choi, M. Lim, S. Choi, H. Kim, J.H. Kwon, K.C. Park, K.C. Choi, A Wearable Photobiomodulation Patch Using a Flexible Red-Wavelength OLED and Its In Vitro Differential Cell Proliferation Effects, Adv. Mater. Technol. 3 (2018) 1–10. https://doi.org/10.1002/admt.201700391.

[3] P.E. Burrows, G. Gu, V. Bulović, Z. Shen, S.R. Forrest, M.E. Thompson, Achieving full-color organic light-emitting devices for lightweight, flat-panel displays, IEEE Trans. Electron Devices. 44 (1997) 1188–1203. https://doi.org/10.1109/16.605453.

[4] S. Grigalevicius, D. Tavgeniene, G. Krucaite, R. Griniene, W.-C. Li, D. Luo, C.-H. Chang, 9,9′-bis(2,2-diphenylvinyl)[3,3′]bicarbazole as low cost efficient hole transporting material for application in red PhOLEDs, Dye. Pigment. 152 (2018) 100–104. https://doi.org/10.1016/j.dyepig.2018.01.040.

[5] L.M. Cosovanu, A. Done, Development of Visible Light Communication System for Automotive Applications Based on Organic Light Emitting Diode Panels, 2020 15th Int. Conf. Dev. Appl. Syst. DAS 2020 - Proc. (2020) 84–89. https://doi.org/10.1109/DAS49615.2020.9108953.

[6] M. Kruppa, W. Thomas, W. Huhn, An OLED taillight revolution: From point light sources to segmented area light sources, Inf. Disp. (1975). 35 (2019) 14–18. https://doi.org/10.1002/msid.1046.

[7] D.Q. Chowdhury, S.M. Garner, S.C. Lewis, Application of OLED for Automotive Lighting, in: 2019 26th Int. Work. Act. Flatpanel Displays Devices, IEEE, 2019: pp. 1–3. https://doi.org/10.23919/AM-FPD.2019.8830593.

[8] C. May, Flexible OLED lighting and signage for automotive application, in: 2021 28th Int. Work. Act. Flatpanel Displays Devices, IEEE, 2021: pp. 42–45. https://doi.org/10.23919/AM-FPD52126.2021.9499164.

[9] K. Blankenbach, Automotive Displays: The Race is on Between LCD and OLED!, Inf. Disp. (1975). 37 (2021) 19–23. https://doi.org/10.1002/msid.1244.

[10] B.N. Patel, M.M. Prajapati, OLED: A Modern Display Technology, Int. J. Sci. Res. Publ. 4 (2014) 1–5. www.ijsrp.org.

[11] M. Sarma, K.T. Wong, Exciplex: An Intermolecular Charge-Transfer Approach for TADF, ACS Appl. Mater. Interfaces. 10 (2018) 19279–19304. https://doi.org/10.1021/acsami.7b18318.

[12] T. Xu, J.G. Zhou, C.C. Huang, L. Zhang, M.K. Fung, I. Murtaza, H. Meng, L.S. Liao, Highly Simplified Tandem Organic Light-Emitting Devices Incorporating a Green Phosphorescence Ultrathin Emitter within a Novel Interface Exciplex for High Efficiency, ACS Appl. Mater. Interfaces. 9 (2017) 10955–10962. https://doi.org/10.1021/acsami.6b16094.

[13] M. Jung, J.Y. Lee, Exciplex hosts for blue phosphorescent organic light-emitting diodes, J. Inf. Disp. 21 (2020) 1–8. https://doi.org/10.1080/15980316.2019.1680453.

[14] Y. Seino, H. Sasabe, Y.J. Pu, J. Kido, High-performance blue

phosphorescent OLEDs using energy transfer from exciplex, Adv. Mater. 26 (2014) 1612–1616. https://doi.org/10.1002/adma.201304253.

[15] C.J. Shih, C.C. Lee, Y.H. Chen, S. Biring, G. Kumar, T.H. Yeh, S. Sen, S.W. Liu, K.T. Wong, Exciplex-Forming Cohost for High Efficiency and High Stability Phosphorescent Organic Light-Emitting Diodes, ACS Appl. Mater. Interfaces. 10 (2018) 2151–2157. https://doi.org/10.1021/acsami.7b15034.

[16] C.J. Shih, C.C. Lee, T.H. Yeh, S. Biring, K.K. Kesavan, N.R. Al Amin, M.H. Chen, W.C. Tang, S.W. Liu, K.T. Wong, Versatile Exciplex-Forming Co-Host for Improving Efficiency and Lifetime of Fluorescent and Phosphorescent Organic Light-Emitting Diodes, ACS Appl. Mater. Interfaces. 10 (2018) 24090–24098. https://doi.org/10.1021/acsami.8b08281.

[17] S.K. Shin, S.H. Han, J.Y. Lee, High triplet energy exciplex host derived from a CN modified carbazole based n-type host for improved efficiency and lifetime in blue phosphorescent organic light-emitting diodes, J. Mater. Chem. C. 6 (2018) 10308–10314. https://doi.org/10.1039/C8TC02918K.

[18] M. Zhang, K. Wang, C.J. Zheng, D.Q. Wang, Y.Z. Shi, H. Lin, S.L. Tao, X. Li, X.H. Zhang, Development of red exciplex for efficient OLEDs by employing a phosphor as a component, Front. Chem. 7 (2019) 1–23. https://doi.org/10.3389/fchem.2019.00016.

[19] N. Altinolcek, A. Battal, M. Tavasli, J. Cameron, W.J. Peveler, H.A. Yu, P.J. Skabara, Yellowish-orange and red emitting quinoline-based iridium(III) complexes: Synthesis, thermal, optical and

electrochemical properties and OLED application, Synth. Met. 268 (2020) 116504. https://doi.org/10.1016/j.synthmet.2020.116504.

[20] T. Fleetham, G. Li, J. Li, Phosphorescent Pt(II) and Pd(II) Complexes for Efficient, High-Color-Quality, and Stable OLEDs, Adv. Mater. 29 (2017) 1–16. https://doi.org/10.1002/adma.201601861.

[21] S. Igawa, M. Hashimoto, I. Kawata, M. Yashima, M. Hoshino, M. Osawa, Highly efficient green organic light-emitting diodes containing luminescent tetrahedral copper(i) complexes, J. Mater. Chem. C. 1 (2013) 542–551. https://doi.org/10.1039/c2tc00263a.

[22] M.C. Tang, C.H. Lee, S.L. Lai, M. Ng, M.Y. Chan, V.W.W. Yam, Versatile Design Strategy for Highly Luminescent Vacuum-Evaporable and Solution-Processable Tridentate Gold(III) Complexes with Monoaryl Auxiliary Ligands and Their Applications for Phosphorescent Organic Light Emitting Devices, J. Am. Chem. Soc. 139 (2017) 9341–9349. https://doi.org/10.1021/jacs.7b04788.

[23] D.R. Lee, J. Lim, J.Y. Lee, Phthalonitrile based charge transfer type host for yellow phosphorescent organic light-emitting diodes, Org. Electron. 94 (2021) 106166. https://doi.org/10.1016/j.orgel.2021.106166.

[24] N.H. Cho, J.Y. Lee, O.Y. Kim, S.H. Hwang, Regioisomer effects of dibenzofuran-based bipolar host materials on yellow phosphorescent OLED device performance, New J. Chem. 44 (2020) 3868–3873. https://doi.org/10.1039/c9nj05249f.

[25] D. Blazevicius, G. Krucaite, S. Shahnawaz, S.S. Swayamprabha, E. Zaleckas, J.H. Jou, S. Grigalevicius, Easily synthesized and cheap carbazole- or phenoxazine-based hosts for efficient yellow

phosphorescent OLEDs, Opt. Mater. (Amst). 118 (2021) 111251. https://doi.org/10.1016/j.optmat.2021.111251.

[26] Q. Mei, R. Sheng, W. Cheng, J. Zhang, P. Wang, Q. Mei, P. Chen, B. Tong, High stability and luminance efficiency thieno[2,3-: D] pyridazine-based iridium complexes and their applications in high-performance yellow OLEDs, Dalt. Trans. 49 (2020) 13797–13804. https://doi.org/10.1039/d0dt02886j.

[27] D. Liu, R. Yao, R. Dong, F. Jia, M. Fu, A strategy to increase phosphorescent efficiency without perturbing emission color for benzothiazole-containing iridium phosphors, Dye. Pigment. 145 (2017) 528–537. https://doi.org/10.1016/j.dyepig.2017.06.048.

[28] B.Y. Ren, R. Da Guo, D.K. Zhong, C.J. Ou, G. Xiong, X.H. Zhao, Y.G. Sun, M. Jurow, J. Kang, Y. Zhao, S.B. Li, L.X. You, L.W. Wang, Y. Liu, W. Huang, A Yellow-Emitting Homoleptic Iridium(III) Complex Constructed from a Multifunctional Spiro Ligand for Highly Efficient Phosphorescent Organic Light-Emitting Diodes, Inorg. Chem. 56 (2017) 8397–8407. https://doi.org/10.1021/acs.inorgchem.7b01034.

[29] K. Guo, S. Wang, C. Si, T. Wang, J. Zhang, C. Chen, Y. Jing, L. Yang, G. Chen, B. Wei, Carrier transfer and luminescence characteristics of thickness-dependent organic light-emitting diodes using transporting material as the host of emitting layer, Phys. Status Solidi Appl. Mater. Sci. 214 (2017) 1–7. https://doi.org/10.1002/pssa.201600689.

[30] J. Kuwabara, T. Namekawa, E. Sakabe, M. aki Haga, T. Kanbara, Luminescent Ir(III) complexes bearing benzothiazole or benzoxazole-

based pincer ligand, J. Organomet. Chem. 845 (2017) 189–195. https://doi.org/10.1016/j.jorganchem.2017.04.037.

[31] B. Liu, F. Dang, Z. Feng, Z. Tian, J. Zhao, Y. Wu, X. Yang, G. Zhou, Z. Wu, W.Y. Wong, Novel iridium(III) complexes bearing dimesitylboron groups with nearly 100% phosphorescent quantum yields for highly efficient organic light-emitting diodes, J. Mater. Chem. C. 5 (2017) 7871–7883. https://doi.org/10.1039/c7tc02369c.

[32] S. Sanderson, B. Philippa, G. Vamvounis, P.L. Burn, R.D. White, Understanding charge transport in Ir(ppy) 3 :CBP OLED films, J. Chem. Phys. 150 (2019) 1–8. https://doi.org/10.1063/1.5083639.

[33] Y. Li, X. Gao, L. Wang, G. Tu, Deep-red organic light-emitting diodes with stable electroluminescent spectra based on zinc complex host material, RSC Adv. 7 (2017) 40533–40538. https://doi.org/10.1039/c7ra06105f.

[34] H. Fukagawa, T. Shimizu, H. Hanashima, Y. Osada, M. Suzuki, H. Fujikake, Highly efficient and stable red phosphorescent organic light-emitting diodes using platinum complexes, Adv. Mater. 24 (2012) 5099–5103. https://doi.org/10.1002/adma.201202167.

[35] V. Adamovich, L. Benavent, P.L.T. Boudreault, M.A. Esteruelas, A.M. López, E. Oñate, J.Y. Tsai, Pseudo-Tris(heteroleptic) Red Phosphorescent Iridium(III) Complexes Bearing a Dianionic C, N, C′, N′-Tetradentate Ligand, Inorg. Chem. 60 (2021) 11347–11363. https://doi.org/10.1021/acs.inorgchem.1c01303.

[36] Y. Ding, D. Liu, J. Li, H. Li, H. Ma, D. Li, R. Niu, Saturated red phosphorescent Iridium(III) complexes containing phenylquinoline ligands for efficient organic light-emitting diodes, Dye. Pigment. 179

(2020) 108405. https://doi.org/10.1016/j.dyepig.2020.108405.

[37] J.-H. Lee, D.N. Liu, S.-T. Wu, Introduction to Flat Panel Displays, 2008.

[38] M. Pope, H.P. Kallmann, P. Magnante, Electroluminescence in organic crystals, J. Chem. Phys. 38 (1963) 2042–2043. https://doi.org/10.1063/1.1733929.

[39] C. Adachi, M.A. Baldo, M.E. Thompson, S.R. Forrest, Nearly 100% internal phosphorescence efficiency in an organic light emitting device, J. Appl. Phys. 90 (2001) 5048–5051. https://doi.org/10.1063/1.1409582.

[40] L. Yao, B. Yang, Y. Ma, Progress in next-generation organic electroluminescent materials: Material design beyond exciton statistics, Sci. China Chem. 57 (2014) 335–345. https://doi.org/10.1007/s11426-013-5046-y.

[41] N.R. Al Amin, K.K. Kesavan, S. Biring, C.C. Lee, T.H. Yeh, T.Y. Ko, S.W. Liu, K.T. Wong, A Comparative Study via Photophysical and Electrical Characterizations on Interfacial and Bulk Exciplex-Forming Systems for Efficient Organic Light-Emitting Diodes, ACS Appl. Electron. Mater. 2 (2020) 1011–1019. https://doi.org/10.1021/acsaelm.0c00062.

[42] M. Matsuoka, M. Saito, M. Anpo, Photoluminescence Spectroscopy, Charact. Solid Mater. Heterog. Catal. From Struct. to Surf. React. Vol. 1&2. 1 (2012) 149–184. https://doi.org/10.1002/9783527645329.ch4.

[43] S. Nowy, W. Ren, J. Wagner, J.A. Weber, W. Brütting, Impedance spectroscopy of organic hetero-layer OLEDs as a probe for charge

carrier injection and device degradation, Org. Light Emit. Mater. Devices XIII. 7415 (2009) 74150G. https://doi.org/10.1117/12.824856.

[44] T. Okachi, T. Nagase, T. Kobayashi, H. Naito, Determination of charge-carrier mobility in organic light-emitting diodes by impedance spectroscopy in presence of localized states, Jpn. J. Appl. Phys. 47 (2008) 8965–8972. https://doi.org/10.1143/JJAP.47.8965.

[45] R. Zheng, W.B. Huang, W. Xu, Y. Cao, Analysis of intrinsic degradation mechanism in organic light-emitting diodes by impedance spectroscopy, Chinese Phys. Lett. 31 (2014) 027703. https://doi.org/10.1088/0256-307X/31/2/027703.

[46] P. Juhasz, J. Nevrela, M. Micjan, M. Novota, J. Uhrik, L. Stuchlikova, J. Jakabovic, L. Harmatha, M. Weis, Charge injection and transport properties of an organic light-emitting diode, Beilstein J. Nanotechnol. 7 (2016) 47–52. https://doi.org/10.3762/bjnano.7.5.

[47] H. Park, H. Kim, S.K. Dhungel, J. Yi, S.Y. Sohn, D.G. Jung, Impedance spectroscopy analysis of organic light-emitting diodes fabricated on plasma-treated indium-tin-oxide surfaces, J. Korean Phys. Soc. 51 (2007) 1011–1015. https://doi.org/10.3938/jkps.51.1011.

[48] S.H. Kim, K.H. Choi, H.M. Lee, D.H. Hwang, L.M. Do, H.Y. Chu, T. Zyung, Impedance spectroscopy of single- and double-layer polymer light-emitting diode, J. Appl. Phys. 87 (2000) 882–888. https://doi.org/10.1063/1.371956.

[49] J.F. Rubinson, Y.P. Kayinamura, Charge transport in conducting polymers: Insights from impedance spectroscopy, Chem. Soc. Rev.

38 (2009) 3339–3347. https://doi.org/10.1039/b904083h.

[50] C.C. Chen, B.C. Huang, M.S. Lin, Y.J. Lu, T.Y. Cho, C.H. Chang, K.C. Tien, S.H. Liu, T.H. Ke, C.C. Wu, Impedance spectroscopy and equivalent circuits of conductively doped organic hole-transport materials, Org. Electron. 11 (2010) 1901–1908. https://doi.org/10.1016/j.orgel.2010.09.005.

[51] S.M. Han, K.P. Kim, D.C. Choo, T.W. Kim, J.H. Seo, Y.K. Kim, Equivalent circuit models in organic light-emitting diodes designed using a cole-cole plot, Mol. Cryst. Liq. Cryst. 470 (2007) 279–287. https://doi.org/10.1080/15421400701495989.

[52] J.H. Lee, S. Lee, S.J. Yoo, K.H. Kim, J.J. Kim, Langevin and trap-assisted recombination in phosphorescent organic light emitting diodes, Adv. Funct. Mater. 24 (2014) 4681–4688. https://doi.org/10.1002/adfm.201303453.

[53] T.H. Han, W. Song, T.W. Lee, Elucidating the crucial role of hole injection layer in degradation of organic light-emitting diodes, ACS Appl. Mater. Interfaces. 7 (2015) 3117–3125. https://doi.org/10.1021/am5072628.

[54] T.H. Han, Y.H. Kim, M.H. Kim, W. Song, T.W. Lee, Synergetic Influences of Mixed-Host Emitting Layer Structures and Hole Injection Layers on Efficiency and Lifetime of Simplified Phosphorescent Organic Light-Emitting Diodes, ACS Appl. Mater. Interfaces. 8 (2016) 6152–6163. https://doi.org/10.1021/acsami.5b11791.

[55] S. Barth, P. Müller, H. Riel, P.F. Seidler, W. Rieß, H. Vestweber, H. Bässler, Electron mobility in tris(8-hydroxy-quinoline)aluminum thin

films determined via transient electroluminescence from single- and multilayer organic light-emitting diodes, J. Appl. Phys. 89 (2001) 3711–3719. https://doi.org/10.1063/1.1330766.

[56] M. Wang, Y.H. Huang, K.S. Lin, T.H. Yeh, J. Duan, T.Y. Ko, S.W. Liu, K.T. Wong, B. Hu, Revealing the Cooperative Relationship between Spin, Energy, and Polarization Parameters toward Developing High-Efficiency Exciplex Light-Emitting Diodes, Adv. Mater. 31 (2019) 1–8. https://doi.org/10.1002/adma.201904114.

[57] C.C. Lee, N.R. Al Amin, J.J. Xu, B.C. Wang, D. Luo, K. Sutanto, S. Biring, S.W. Liu, C.H. Chen, Structural effect of phenylcarbazole-based molecules on the exciplex-forming co-host system to achieve highly efficient phosphorescent OLEDs with low efficiency roll-off, J. Mater. Chem. C. 9 (2021) 9453–9464. https://doi.org/10.1039/d1tc02290c.

[58] W.Y. Hung, P.Y. Chiang, S.W. Lin, W.C. Tang, Y.T. Chen, S.H. Liu, P.T. Chou, Y.T. Hung, K.T. Wong, Balance the Carrier Mobility to Achieve High Performance Exciplex OLED Using a Triazine-Based Acceptor, ACS Appl. Mater. Interfaces. 8 (2016) 4811–4818. https://doi.org/10.1021/acsami.5b11895.

[59] Y. Kawamura, K. Goushi, J. Brooks, J.J. Brown, H. Sasabe, C. Adachi, 100% phosphorescence quantum efficiency of Ir (III) complexes in organic semiconductor films, Appl. Phys. Lett. 86 (2005) 1–3. https://doi.org/10.1063/1.1862777.

[60] Z. Gao, F. Wang, K. Guo, H. Wang, B. Wei, B. Xu, Carrier transfer and luminescence characteristics of concentration- dependent phosphorescent Ir(ppy)3 doped CBP film, Opt. Laser Technol. 56

(2014) 20–24. https://doi.org/10.1016/j.optlastec.2013.07.011.

[61] Z.L. Jiang, W. Tian, Z.Q. Kou, S. Cheng, Y.H. Li, The influence of the mixed host emitting layer based on the TCTA and TPBi in blue phosphorescent OLED, Opt. Commun. 372 (2016) 49–52. https://doi.org/10.1016/j.optcom.2016.04.002.